Discovery of novel akt1 inhibitor induces autophagy associated death in hepatocellular carcinoma cells

Meng Yu, Minghui Zeng, Zhaoping Pan, Fengbo Wu, Li Guo, Gu He

PII: S0223-5234(20)30043-X

DOI: https://doi.org/10.1016/j.ejmech.2020.112076

Reference: EJMECH 112076

To appear in: *European Journal of Medicinal Chemistry*

Received Date: 12 November 2019

Revised Date: 8 January 2020

Accepted Date: 15 January 2020

Please cite this article as: M. Yu, M. Zeng, Z. Pan, F. Wu, L. Guo, G. He, Discovery of novel akt1 inhibitor induces autophagy associated death in hepatocellular carcinoma cells, *European Journal of Medicinal Chemistry* (2020), doi: https://doi.org/10.1016/j.ejmech.2020.112076.

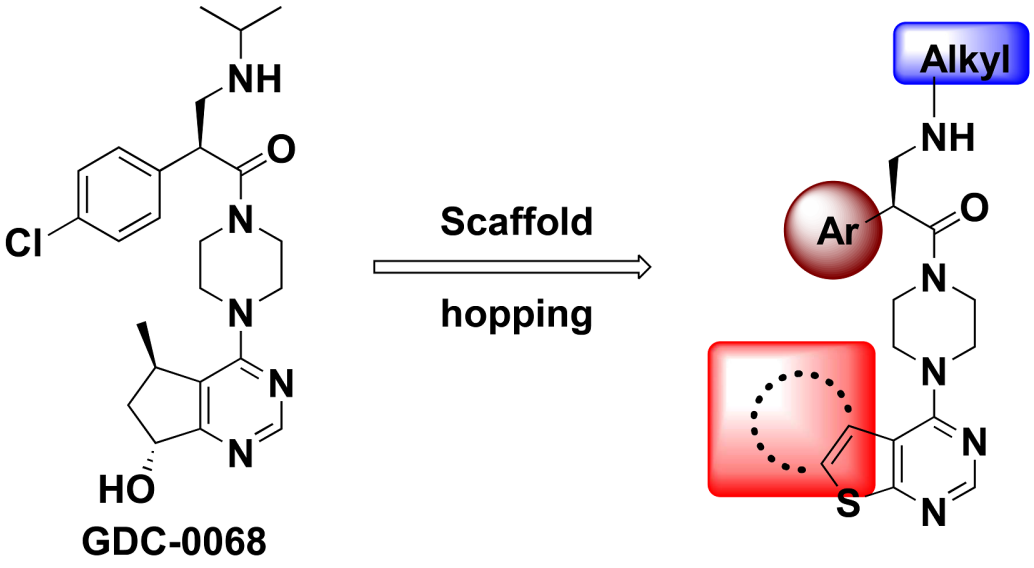

GDC-0068

Novel Akt inhibitor induces autopahgic associated death in HCC cells

Discovery of novel akt1 inhibitor induces autophagy associated death in hepatocellular carcinoma cells

Meng Yu,[1,2,†] Minghui Zeng,[3,†] Zhaoping Pan,[2] Fengbo Wu,[2] Li Guo[1,*] and Gu He[2,*]

1 Department of Medicinal Chemistry, West China School of Pharmacy, Sichuan University, Chengdu, Sichuan 610041, PR China

2 State Key Laboratory of Biotherapy and Cancer Center, West China Hospital, Sichuan University and Collaborative Innovation Center of Biotherapy, Chengdu, Sichuan 610041, PR China

3 Department of Pharmacy, Qionglai Medical Center Hospital of Sichuan Province, Chengdu, Sichuan 611500, PR China

† These authors contributed equally to this work.

Abstract

In this study, a series of thieno[2,3-d]pyrimidine derivatives were designed, synthesized and evaluated as novel AKT1 inhibitors. In vitro antitumor assay results showed that compounds 9d-g and 9i potently suppressed the enzymatic activities of AKT1 and potently inhibited the proliferation of HepG2, Hep3B, Huh-7 and SMMC-7721 cancer cell lines. Among these derivatives, the compound 9f demonstrated the best inhibitory activities on AKT1 (IC50 = 0.034μM) and Huh-7 cell (IC50 = 0.076μM). A panel of biological assays showed that compound 9f suppressed the cellular proliferation of Huh-7 through Akt/mTOR signaling pathway mediated autophagy mechanism. Furthermore, the antitumor capacity of 9f was validated in the subcutaneous Huh-7 xenograft models. Together, our results demonstrate that a novel small-molecule Akt1 inhibitor induces autophagy associated death in hepatocellular carcinoma, which may afford a potential drug candidate for targeted cancer therapy.

Keywords: hepatocellular carcinoma, Akt1, inhibitor, autophagy

1. Introduction

Hepatocellular carcinoma (HCC) is a malignant tumor with a high incidence worldwide.[1-3] It is closely related to liver diseases arising from viral infection, such as hepatitis B virus (HBV) and hepatitis C virus (HCV), alcoholic liver disease, toxic substances, parasites, heredity and aflatoxin, etc.[4] Currently, the main clinical care include surgery, intervention, ablation, targeted drugs, radiotherapy and other methods according to the stage of the tumor; however, they all have limited efficacy.[5-7]

AKT, also known as protein kinase B (PKB), is a Ser/Thr kinase with high homology to PKA and PKC, belongs to AGC kinases family. Akt includes three closely related isoforms, comprising Akt1, Akt2, and Akt3, and these three isoforms share more than 80% sequence identity and similar downstream targets.[8-10] It plays a key role in many cell growth processes, such as glucose metabolism, apoptosis, cell proliferation, transcription and cell migration.[11, 12] It is over expressed and / or over activated in many tumor cells.[13] This abnormally high expression of Akt in cancer,[14] can be used to design therapeutics against it for restraining the growth and progression of the tumor. It can be used alone as a therapeutic or in combination with other chemotherapeutics.[15-17] Nowadays, there are several Akt inhibitors, which are undergoing clinical trials for efficacy **(Figure 1 and Table S1)**. Many immunotherapies have been in development for different types of cancers. Particularly, Ipatasertib (GDC-0068) is currently in a phase-II study to check its efficacy as a monotherapy for the treatment of triple-negative breast cancer (TNBC).[18] Further, the use of AZD5363 in combination with paclitaxel to treat triple-negative breast cancer has also been reported, which demonstrates that this

treatment can prolong the overall survival of patients significantly and improve their quality of life.[19] Another drug, GSK690693 which has been used to treat acute lymphoblastic leukemia clinically, has been withdrawn due to some adverse reactions, like hyperglycemia.[20]

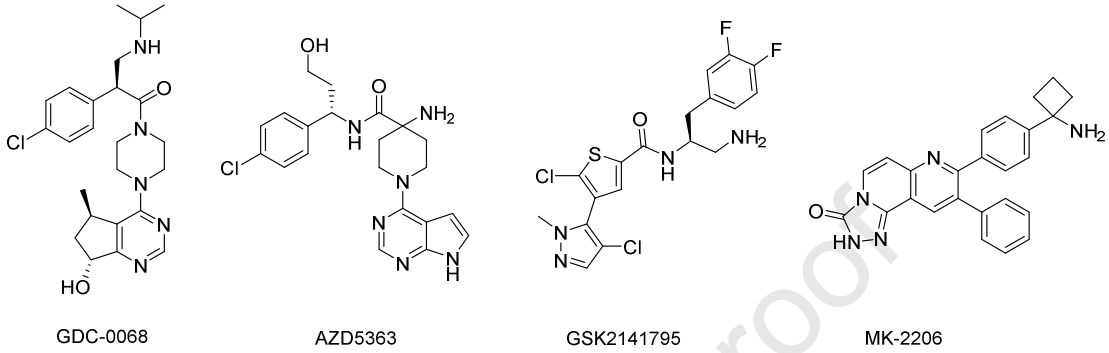

Figure 1. Chemical structures of representative Akt1 inhibitors.

GSK2141795 (Uprosertib), a ATP competitive Akt inhibitor, which is used as a therapeutic in different types of cancer (such as melanoma, breast cancer, etc).[21] Another monotherapy, MK-2206 used against for the clinical management of myelogenous leukemia, has only limited topical use as the patients experienced hemolytic toxicity after intravenous injection.[22] Therefore, this indicates that Akt inhibitors might have broad application prospects as anticancer drugs.

In the current study, we have investigated the structured-based design, synthesis and in vitro mechanistic studies of thieno[2,3-d]pyrimidine based Akt1 inhibitors. The substituted phenylalanine amino acids was linked to the thieno[2,3-d]pyrimidine scaffold resulting in better kinase inhibition. The *in vitro* kinase inhibition and selectivity assays, cell proliferation, apoptosis and autophagy assays were measured to understand the molecular mechanisms of these novel Akt1 inhibitors. The results suggests that the novel Akt1 inhibitor **9f** suppress the activation of the PI3K/Akt/mTOR signaling pathway and cellular proliferation in human HCC cells.

Furthermore, **9f** induces autophagy and apoptotosis of the HCC cells. This suggests novel molecular mechanism of these Akt inhibitors which needs to be studied further for the development of more efficient therapeutics.

2. Results and discussion

Akt1 is hyperactivated in hepatocellular carcinoma

The mRNA-sequencing data of the hepatocellular carcinoma cohort in TCGA (The Cancer Genomics Atlas) database showed that there was no significant difference on the Akt1 mRNA levels between the cancer and the normal tissues (**Figure 2A**).[23-25] However, the expression level of Akt1 was a significant prognostic factor for both, overall survival ($p = 0.013$, HR = 1.6) and disease-free survival ($p < 0.01$, HR = 1.6) of the HCC patients (**Figure 2B and 2C**). Moreover, the IHC images in ProteinAtlas database suggests that the Akt1 protein levels were not changed in both the HCC tissues and the adjacent normal tissues (ANT).[26] As there was no significant difference in the mRNA and protein levels of Akt1 in the HCC and the ANT tissues, we speculated that it was probably hyperactivated in the HCC tissues. Therefore, we performed IHC analysis of phosphorylated antibody of Akt1 (Ser473) on a HCC tissue microarray. As shown in **Figure 2D** and **Table S2** the pAkt1 (Ser473) levels in HCC tissues were remarkably higher than that of adjacent normal tissues, and the expression profiles of pAkt1 (Ser473) were significantly related to the primary tumor stage, regional lymph nodes and distant metastasis.[27-29] Thus, from this results, we hypothesize that the hyperactivated Akt1 might be a potential therapeutic target in HCC.

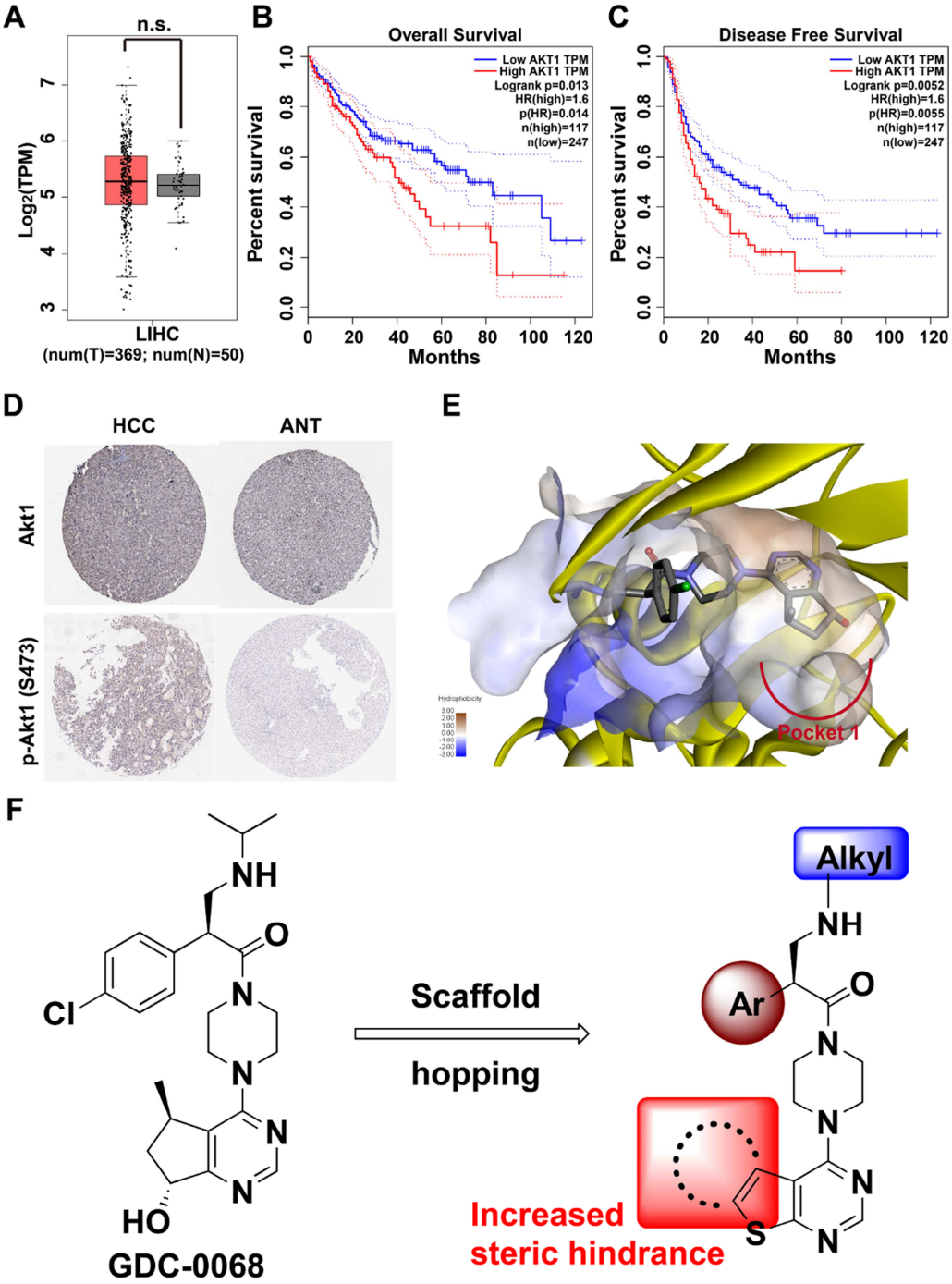

Figure 2. (A) The Akt1 mRNA expression levels of HCC and normal liver tissues in TCGA database; The Kaplan-Meier plots of overall survival (B) and disease-free survival (C) ratio in HCC cohort of TCGA database; (D) The protein expression levels of total Akt1 and p-Akt1(S473) in HCC and adjacent normal tissues by IHC; (E) The 3D contour of the binding mode of GDC-0068 in ATP site of Akt1; (F) The scaffold hopping strategy of novel Akt1 inhibitors.

Design and Synthesis of novel Akt1 Inhibitors.

There were many Akt1 inhibitors reported with diverse structural scaffold, however, the kinase selectivity of some Akt1 inhibitors remained limited. We utilized protein kinase A (PKA), a highly homology proteins of Akt1, to analyze the specific binding mechanisms of Akt1.[30, 31] After aligned and superposed the crystallized structures of PKA and Akt1 together (**Figure S1A**), we could find that they were very similar to each other. The only difference between the ATP sites of PKA and Akt1 was depicted in **Figure 2E** and **Figure S1B and S1C**. The steric tolerance in the ATP site of Akt1 was higher than that of PKA, which was also validated by the previous reported SAR analysis of GDC-0068 analogues. Therefore, at the hand of rational drug design strategy, we proposed to change we a thieno[2,3-*d*]pyrimidine based tricycle scaffold as the core structure to replace the cyclopenta[*d*]pyrimidine scaffold of GDC-0068 or pyrrolo[2,3-*d*]pyrimidine scaffold of AZD5363.[32-35] The α-substituted phenylacetyl piperidine group, serving as key pharmacophore, were retained and variants at 4-position of pyrimidine ring could enrich the diversity in the drug-like skeleton. The resulting compounds may serve as the basis for exploring novel and efficient Akt1 inhibitors (Figure **2F**).

The synthesis routes of the compounds **5a-o, 9a-k, and 13** are shown in **Scheme 1-3**. The synthesis of thieno[2,3-d]pyrimidine derivatives **2a-f** followed our established methods.[36, 37] Briefly, we used N-substituted piperidinones and an α-cyanoester as raw materials to synthesize 2-aminothiophenes by the Gewald synthesis in the presence of rhombic sulfur and a base.[38, 39] Next, these intermediates were incubated in formamidine acetate in DMF for 12 hours at 100°C to obtain a crystal (**2a-f**) requiring no further purification**,** and then the compounds **2a-f**

were converted to an intermediate form, 4-chloro-pyrimidines by treatment with $POCl_3$. The piperazine analogue **3a-f** was synthesized through the S_NAr reaction using the commercially available N-Boc piperazine and 4-chloro-pyrimidines under alkaline condition in NMP as outlined (**Scheme 1**) to afford the N-Boc piperazine intermediate crystals requiring no further purification, after that the standard trifluoroacetic acid-based N-Boc de-protection reaction was followed to obtain **3a-f**.[40] The substituted phenylalanine amino acids derivatives **4a-j** was synthesized through four steps, as shown in **Scheme S1**. In the first stage, phenyl acetate esters were converted to the acrylates as previously reported.[41] Then through Michael addition of amines following by N-Boc protection and hydrolysis of the methyl ester, the compound **4a-j** was obtained for overall yield of 13-17%. With the essential thieno[2,3-*d*]pyrimidine scaffolds and phenylalanine acids derivatives **4a-j** in hand, the synthesis of the target compounds **5a-o** was completed by amide coupling under the presence of the peptide coupling agent HATU, followed by the N-Boc de-protection under acid conditions, as shown in **Scheme 1**. Similarly, we used cyclohexanone, cyclopentanone and tetrahydropyranone (**8a-c**) as raw materials to synthesize the compounds **9a-k** through the same steps as above (**Scheme 2**).

The preparation of the compound **13** is shown in **Scheme 3**. We choose N-Boc-4-piperidone **10** as the starting materials with similar reaction conditions to synthesize the compound **11**, followed by the N-Boc de-protection of **11** in the presence of trifluoroacetic acid and the obtained compound was treated with dimethylcarbamoyl chloride under the presence of DMAP as a catalyst.[42] Then through the same S_NAr reaction with N-Boc piperazine, N-Boc de-protection and amide coupling with compound **4j,** as above in **Scheme 1**, we finally synthesized the target compound **13**. The synthesized target compounds were characterized by ^1H

NMR, ^{13}C NMR and HR-MS (high-resolution mass spectrometry) and the detailed experimental operation, process and characterization are shown in the experimental sections.

Table 1. The remained kinase activities (%) after 1μM compounds 5a-f, 9a-c and 13 incubation on Akt1-3 and PKA.

No.	X	n	R_1	R_2	R_3	% control[a] @ 1μM			
						PKA(h)	Akt1(h)	Akt2(h)	Akt3(h)
5a	-	-	CH_3	4-Cl	i-Pr	72	50	91	69
5b	-	-	Et	4-Cl	i-Pr	87	73	82	71
5c	-	-	n-Pr	4-Cl	i-Pr	88	75	89	79
5d	-	-	Bn	4-Cl	i-Pr	80	71	77	71
5e	-	-	cyclopropyl	4-Cl	i-Pr	92	77	71	70
5f	-	-	isopropyl	4-Cl	i-Pr	84	76	81	78
9a	CH_2	1	-	4-Cl	i-Pr	78	55	72	63
9b	CH_2	0	-	4-Cl	i-Pr	45	11	57	19
9c	O	1	-	4-Cl	i-Pr	78	78	81	77
13	-	-	-	-	-	80	86	95	87

[a] % control = kinase activity remained.

Scheme 1. Synthesis of compound **5a-o**.

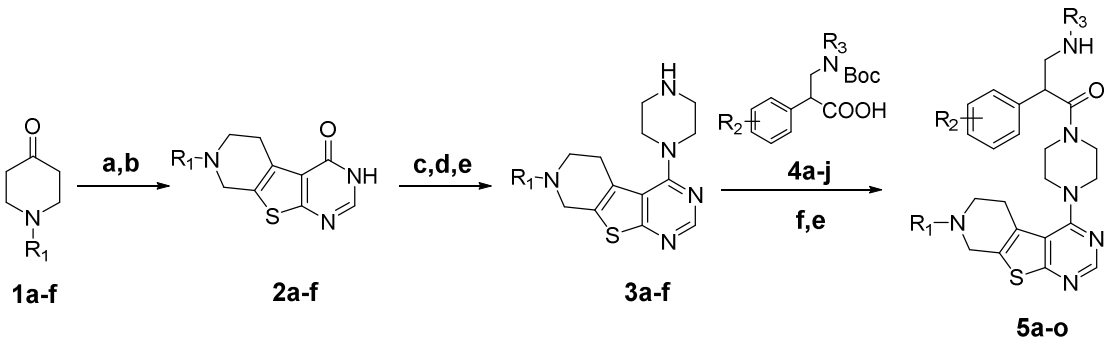

Reagents and conditions: (a) $NCCH_2CO_2Et$, S_8, EtOH, Et_3N, reflux, 12h; (b) formamidine acetate, DMF 100 °C, 1h; (c) $POCl_3$, DIPEA, toluene, 80 °C, overnight; (d) 1-Boc-piperazine, DIPEA, NMP; (e) TFA/DCM, room temperature, 30mins; (f) HATU, ET_3N, DCM.

Scheme 2. Synthesis of compound **9a-k**.

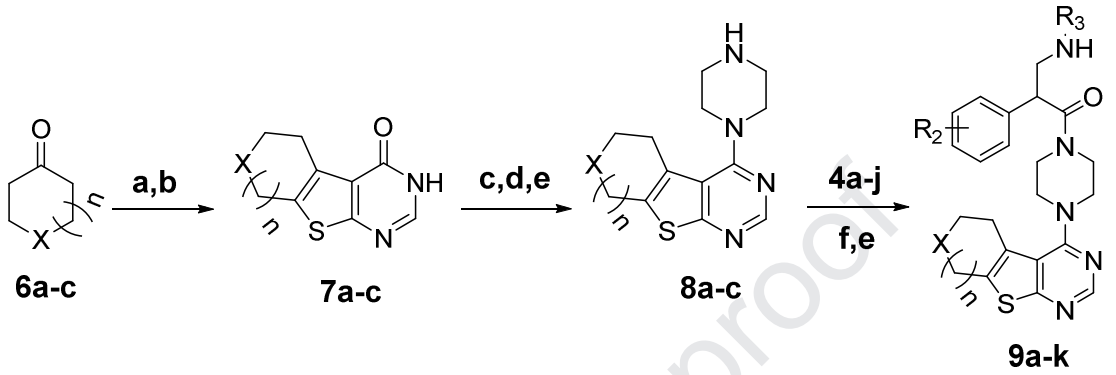

Reagents and conditions: (a) $NCCH_2CO_2Et$, S_8, EtOH, Et_3N, reflux, 12h; (b) formamidine acetate, DMF 100 °C, 1h; (c) $POCl_3$, DIPEA, toluene, 80 °C, overnight; (d) 1-Boc-piperazine, DIPEA, NMP; (e) TFA/DCM, room temperature, 30mins; (f) HATU, ET_3N, DCM.

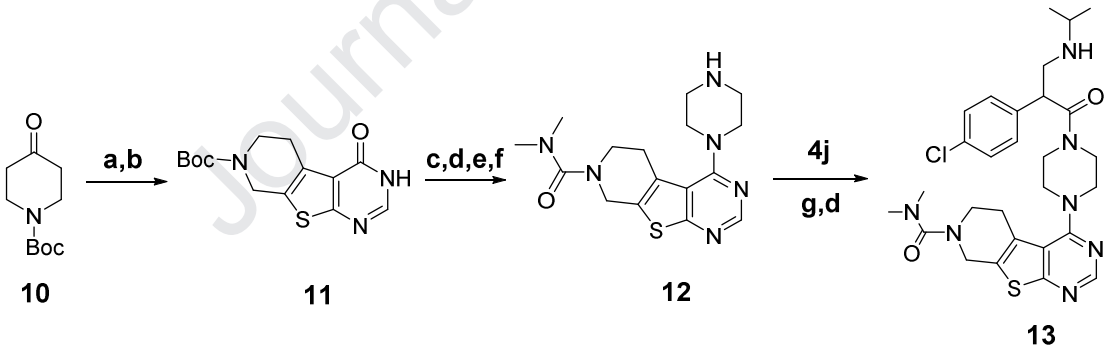

Reagents and conditions: (a) $NCCH_2CO_2Et$, S_8, EtOH, Et3N, reflux, 12h; (b) formamidine acetate, DMF 100 °C, 1h; (c) $POCl_3$, DIPEA, toluene, 80 °C, overnight; (d) TFA/DCM, room temperature, 30mins; (e) dimethylcarbamoyl chloride, pyridine, DMAP, DMSO, 23 °C, 16h; (f) 1-Boc-piperazine, DIPEA, NMP; (g) HATU, ET_3N, DCM.

2.4 The SAR (structure-activity relationship) analysis and binding modes of novel Akt1 inhibitors

The kinase inhibitory abilities of the compounds **5a-o, 9a-k, and 13** are shown in **Table 1** and **2**, including the percentage of the 1.0 μM inhibitor incubated Akt1, Akt2, Akt3 and PKA kinase activity. **Table 1** shows the comparison between the bioactivities of the different ring types that fuse to the thieno[2,3-d]pyrimidine scaffold. The results of the kinase inhibitory assays suggest that a bigger steric volume is an unfavorable to all kinase inhibitory assays, and Akt1 and Akt3 have relatively lower sensitivity than that of PKA. Only two compounds, **5a** and **9b** could suppress half or more of the Akt1 kinase activities at 1.0 μM. The other compounds in **Table 1** with larger substitution to pocket 1, resulted in only marginal inhibition of PKA and Akts, depicting low kinase selectivity. We further optimized the substituted groups on the phenylacetyl piperidine fragment based on the cyclopenta[4,5]thieno [2,3-d]pyrimidine scaffold of **9b** and N-methyl-pyridothieno[2,3-d]pyrimidine scaffold of **5a** (**Table 2**) and observed that any changes to the R_2 or R_3 groups on the N-methyl-pyridothieno[2,3-d]pyrimidine scaffold resulted in a loss of the kinase inhibition activities. For the cyclopenta[4,5]thieno[2,3-d]pyrimidine scaffold, the larger substituted groups on R_3 group is favorable, 4-Cl and 4-Br substitution on R_2 group is favorable, while the ortho-substitution on the R_2 group could diminish the kinase inhibitory activities. Compounds **9d-g** and **9i** almost totally suppressed the kinase activity of Akt1 at 1.0μM concentration. The IC_{50} values of these compounds on Akt1, Akt2 and Akt3, and the IC_{50} of cellular proliferation on HCC cell lines HepG2, Hep3B, Huh-7 and SMMC-7721 are listed in **Table 3**. Compound **9f** demonstrated the best inhibitory activities on Akt1, Akt2 and Akt3 with IC_{50} value of

0.034, 1.709 and 0.129μM, respectively. And all the five compounds exhibit potent cellular proliferation inhibitory capacities on the HCC cell line. The Huh-7 cell is relatively more sensitive than the other cell lines, with an IC_{50} value of 0.076, 0.159 and 0.112 μM to **9f**, **9g** and **9i**, respectively. Moreover, the pan-cancer kinase profiling of compound **9f** was performed to identify its selectivity to a panel of 104 kinases by the KINOMEscan® method. As listed in **Table S3,** with 1.0 μM concentration of the inhibitor, only Akt1 was totally suppressed while the other kinases showed over 40% activity. Thus, compound **9f** was selected for further studies to understand its role in the involved molecular mechanism of the novel AKT1 induced autophagy in the hepatocellular carcinoma with in vivo xenograft evaluations.

Table 2. The remained kinase activities (%) after 1μM compounds 5g-o and 9d-k incubation on Akt1-3 and PKA.

No.	X	n	R_1	R_2	R_3	% control[a] @ 1μM			
						PKA(h)	Akt1(h)	Akt2(h)	Akt3(h)
5g	-	-	CH_3	4-Cl	Et	91	95	107	74
5h	-	-	CH_3	4-Cl	n-Bu	81	81	93	84
5i	-	-	CH_3	4-Cl	Cyclopentyl	82	82	81	76
5j	-	-	CH_3	4-Cl	Cyclohexyl	95	84	88	69
5k	-	-	CH_3	4-F	i-Pr	97	88	111	87
5l	-	-	CH_3	4-Br	i-Pr	88	69	86	72
5m	-	-	CH_3	4-Me	i-Pr	90	78	73	73
5n	-	-	CH_3	4-OMe	i-Pr	95	81	78	76
5o	-	-	CH_3	2-Cl	i-Pr	86	96	83	76
9d	CH_2	0	-	4-Cl	Et	31	1	58	21
9e	CH_2	0	-	4-Cl	n-Bu	37	1	56	15

9f	CH_2	0	-	4-Cl	Cyclopentyl	35	1	63	22
9g	CH_2	0	-	4-Cl	Cyclohexyl	29	1	51	11
9h	CH_2	0	-	4-F	i-Pr	77	26	104	45
9i	CH_2	0	-	4-Br	i-Pr	23	1	67	20
9j	CH_2	0	-	4-OMe	i-Pr	66	18	86	42
9k	CH_2	0	-	2-Cl	i-Pr	95	88	101	92

[a] % control = kinase activity remained.

Table 3. The IC_{50} values (μM) of compounds 9d-g and 9i on Akt1-3 and HCC cell lines.

No.	Kinase activities (IC_{50}, μM)[a]			Anti-proliferative activities(IC_{50}, μM)[b]			
	Akt1	Akt2	Akt3	HepG2	Hep3B	Huh-7	SMMC-7721
9d	0.125±0.019	3.05±0.31	0.101±0.008	0.580±0.068	0.541±0.084	0.283±0.029	1.249±0.12
9e	0.166±0.022	3.78±0.54	0.137±0.011	0.914±0.077	0.833±0.120	0.367±0.057	1.354±0.19
9f	0.034±0.003	1.71±0.18	0.129±0.010	0.183±0.019	0.131±0.014	0.076±0.010	0.386±0.05
9g	0.051±0.006	1.30±0.21	0.045±0.007	0.386±0.040	0.294±0.025	0.159±0.026	0.978±0.08
9i	0.039±0.005	1.36±0.16	0.095±0.011	0.202±0.018	0.228±0.026	0.112±0.009	0.521±0.05
GDC-0068	0.019±0.006	0.032±0.04	0.026±0.007	0.268±0.037	0.389±0.041	0.167±0.018	0.661±0.14

[a] IC_{50} values for enzymatic inhibition of Akt1-3; Data displayed is the average of at least three independent replicates ± standard deviation; IC_{50} values were determined from KinaseProfiler of Eurofins.

[b] IC_{50} = compound concentration required to inhibit tumor cell proliferation by 50%; Data displayed is the average of at least three independent replicates ± standard deviation.

The 3D and 2D contours of compound **9f** bound to the ATP sites of Akt1 are shown in **Figure 3A** and **3B**, respectively. It can be observed that the N1 and S atoms of the thieno[2,3-*d*]pyrimidine ring form stable hydrogen bonds with the Ala230 residue, and the nitrogen atom of the cyclopentamine group forms a hydrogen bond

with Lys158 and electrostatic interaction to Glu278 of Akt1. Moreover, the cyclopenta[*d*]thieno[2,3-*d*]pyrimidine fragment could form hydrophobic interactions with the inner pocket of Akt1, including Met281 and Lys159, which might be a potential reason of kinase selectivity of the compound 9f to Akt1 to the other kinases.

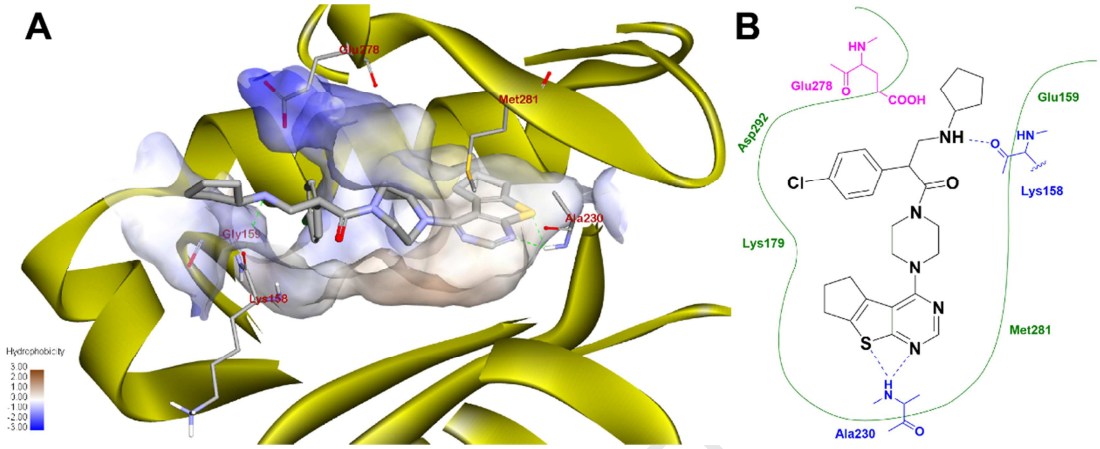

Figure 3. The 3D contour (A) and 2D contour (B) of the binding mode of compound 9f in ATP site of Akt1.

2.5 Novel Akt1 inhibitor induces lethal autophagy in HCC cells

The cytotoxicity assay showed that the compound **9f** suppress the cellular proliferation of a panel of HCC cell lines at submicromolar levels. The potential cell death subroutines of the Huh-7 cells under **9f** incubation were determined by apoptosis and autophagy assays. These include the Annexin-V/PI dual-staining apoptosis assay, GFP-LC3 transfected autophagic puncta assay, as well as the western blotting of the apoptosis and the autophagy related proteins (**Figure 4**). It was observed that **9f** remarkably induced apoptosis of the Huh-7 cells in a dosage-dependent manner, and the number of the autophagosome puncta also increased with **9f** incubation in both Huh-7 and Hep3B cells (Figure 4B and S2).[43-46] WB analysis demonstrates that **9f** treatment declined the phosphorylation levels of Akt1 and GSK3β without interfering with the protein expression of total Akt1 and GSK3β; however, the expression of Bcl-2, an apoptosis inhibitor, was

suppressed after **9f** incubation. To further detect the influence of autophagy flux of 9f incubation, the mCherry-GFP-LC3 plasmid was transfected into Huh-7 cells, and there were massive autophagy puncta formed after 0.2μM 9f incubation (**Figure 4E**).

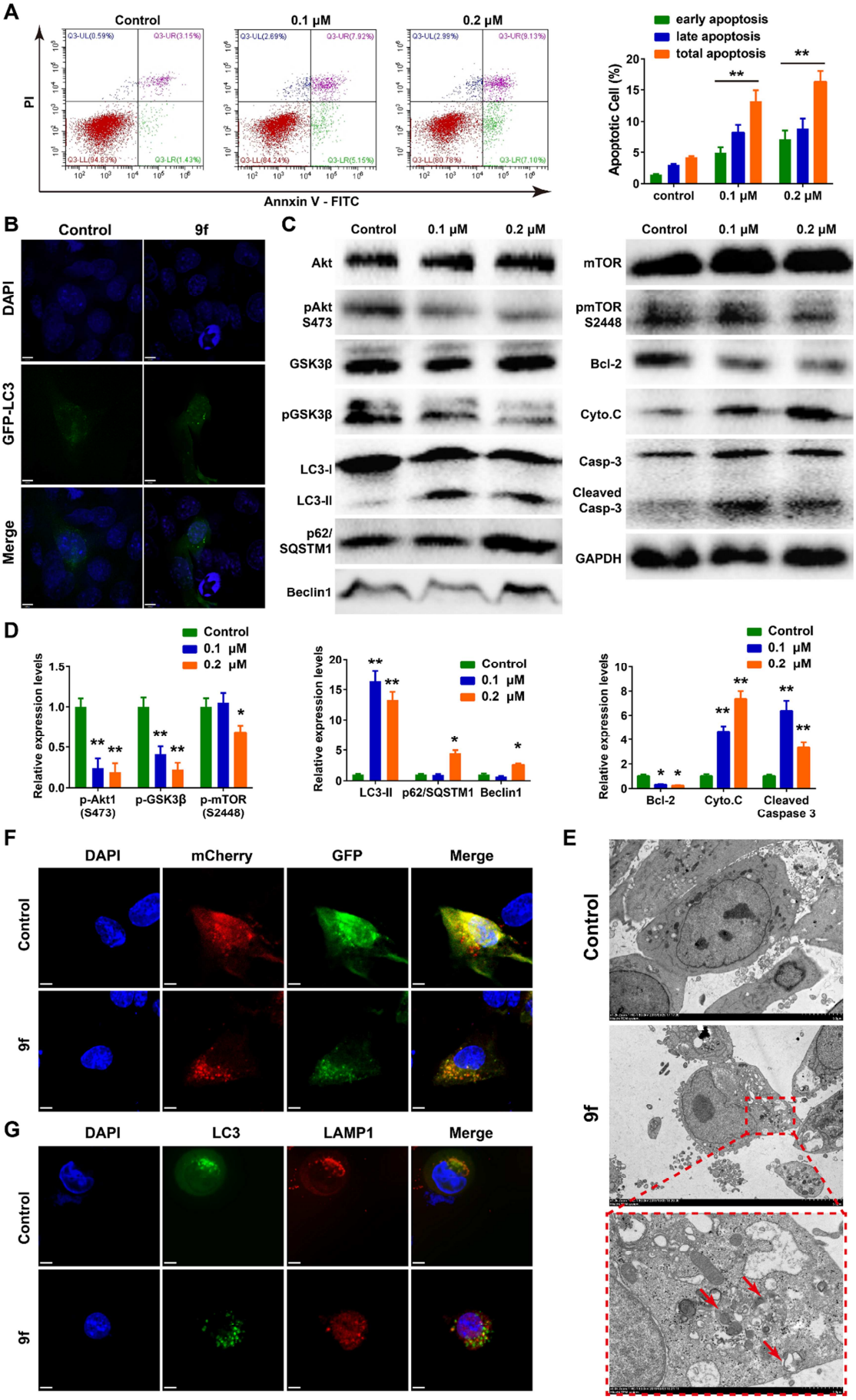
A
Control
0.1 μM
0.2 μM
PI
Annxin V - FITC
Q3-UL(0.59%)
Q3-UR(3.15%)
Q3-LL(94.83%)
Q3-LR(1.43%)
Q3-UL(2.69%)
Q3-UR(7.92%)
Q3-LL(84.24%)
Q3-LR(5.15%)
Q3-UL(2.99%)
Q3-UR(9.13%)
Q3-LL(80.78%)
Q3-LR(7.10%)
early apoptosis
late apoptosis
total apoptosis
Apoptotic Cell (%)
control
0.1 μM
0.2 μM
B
Control
9f
DAPI
GFP-LC3
Merge
C
Control
0.1 μM
0.2 μM
Akt
pAkt S473
GSK3β
pGSK3β
LC3-I
LC3-II
p62/ SQSTM1
Beclin1
mTOR
pmTOR S2448
Bcl-2
Cyto.C
Casp-3
Cleaved Casp-3
GAPDH
D
Control
0.1 μM
0.2 μM
Relative expression levels
p-Akt1 (S473)
p-GSK3β
p-mTOR (S2448)
LC3-II
p62/SQSTM1
Beclin1
Bcl-2
Cyto.C
Cleaved Caspase 3
F
DAPI
mCherry
GFP
Merge
Control
9f
G
DAPI
LC3
LAMP1
Merge
Control
9f
E
Control
9f

Figure 4. (A) The apoptosis in Huh-7 cells induced by compound 9f detected by Annexin V/PI dual staining; (B) The formation of autophagosome in GFP-LC3 transfected Huh-7 cells induced by 0.2μM 9f, Scale bar: 6 μm; (C) Western blotting of proteins associated in Akt/mTOR signaling pathway, apoptosis and autophagy with or without compound 9f incubation; (D) The quantitative analysis of differential expression proteins in western blotting; (E) The TEM images of Huh-7 cells with or without compound 9f incubation,Scale bar: 5.0 μm; (F) The fluorescent images of mCherry-GFP-LC3 plasmid transfected Huh-7 cells induced by 0.2μM compound 9f, Scale bar: 6 μm; (G) The co-localization analysis of LC3 and LAMP1 in Huh-7 cells with or without 0.2μM 9f incubation, Scale bar: 6 μm; *, $P < 0.05$; **, $P < 0.01$.

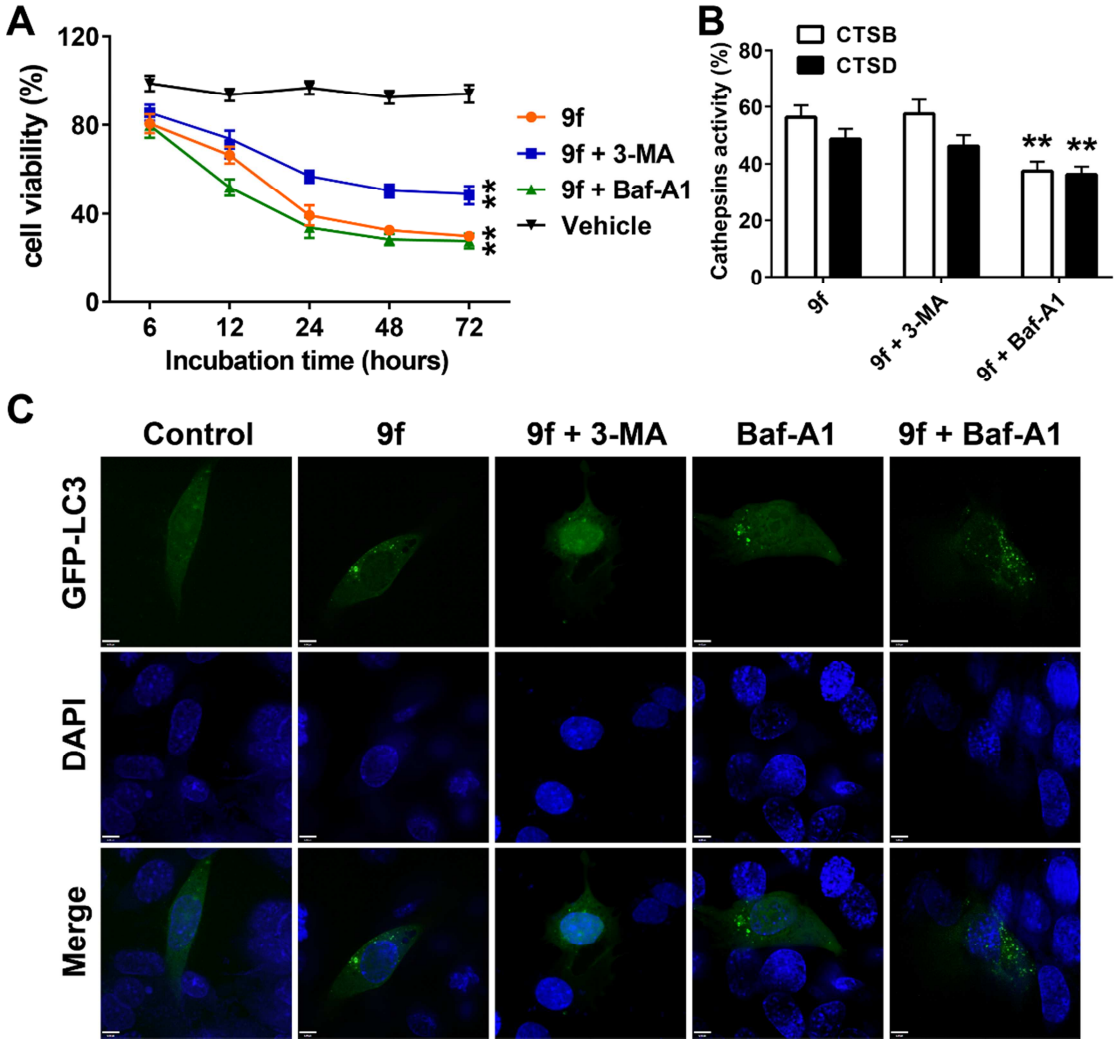

Figure 5. (A) The cell viabilities of Huh-7 cell after incubation with compound 9f and/or autophagy inhibitors; (B) The intracellular Cathepsin B/D activities after incubation with 0.2μM 9f and/or autophagy inhibitors; (C) The accumulation of autophagosomes in GFP-LC3 transfected Huh-7 cells induced by 0.2μM 9f and autophagy inhibitors. Scale bar: 6 μm; **, $P < 0.01$.

Upregulation in the expression of cytochrome C and cleaved caspase-3 were observed after **9f** treatment, which suggests that the compound **9f** triggers the mitochondrial apoptosis pathway, as shown by the increased levels of LC3-II and declined levels of p-mTOR indicating the initiation of the autophagic flux after the **9f** incubation. It is surprising that the **9f** induced accumulation of p62/SQSTM1, a marker of protein digestion by autopahgolysosome, is observed. The autophagy flux arrest by 9f incubation was also confirmed by the immunofluorescent staining of LC3 and LAMP1, a marker of lysosome (**Figure 4F**). The fusion of autophagosome (stained by LC3) and lysosome (stained by LAMP1) was suppressed by 9f treatment. In addition, there was slightly autophagy flux arrest observed after GDC-0068 incubation (Figure S3). In support of our observation, there are several other reports about the Akt1 allosteric inhibitor MK2206 triggered cytoprotective autophagy in the melanoma and the HCC cells.[47-49] We further determined the potential biological functions of the **9f**-induced autophagy by addition of the autophagy inhibitor 3-MA and bafilomycin-A1 (Baf-A1), which 3-MA decreased the cytotoxicity of **9f**; Baf-A1 displayed a synergistic effect to the compound **9f** in Huh-7 cells (**Figure 5A**). The activity assays of cathepsin B and cathepsin D suggests that Baf-A1 suppressed the activities of cathepsins rather than 3-MA (**Figure 5B**). These results suggest that **9f** induces the initiation of autophagosome and disrupts the autophagic flux. Moreover, the fluorescent microscopy images of the GFP-LC3 transfected Huh-7 cells indicate

that the addition of 3-MA inhibited the formation of the autophagosome induced by **9f**, and there was accumulation of autophagosomes after Baf-A1 incubation (**Figure 5C**). The potential signaling pathway involved in the crosstalk between Akt1 inhibition by **9f** and autophagic flux regulation were studied further.

2.6 In vivo xenograft models

A subcutaneous xenograft model of the Huh-7 cells in nude mice was established to investigate the antitumor effect of **9f** *in vivo*. As shown in Figure 6A, intraperitoneal administration of 25 or 50mg/Kg **9f** significantly suppressed the growth of the Huh-7 xenografts ($p < 0.01$). The average weight of the tumor tissues of the treatment group was significantly lower than that of the control group (Figure 6B). The inhibition potentials of the xenograft tumor volume and weight in the 25mg/Kg **9f**-treated group are slightly lower than those of the 50mg/Kg treated group. Moreover, there were no significant changes of the body weight of mice in both the **9f**-treated and control groups. As shown in Figure 6C, we used immunofluorescence and IHC to analyze the tumor tissues further to verify whether the tumor growth suppression regulated by **9f** was related to the inhibition of Akt1 and the apoptosis/autophagy related signaling pathways. The number of the apoptotic positive cells determined by TUNEL staining of the **9f**-treated tumors was significant. In addition, the IHC analysis showed that the phosphorylated levels of Akt decreased, and there was no significant difference between the total Akt levels. The expression levels of the proliferative marker Ki-67 and the autophagy marker p62/SQSTM1 declined, however, the expression of LC3-II elevated. The results of these in vivo experiments demonstrate that **9f** exhibits inhibitory effects on Akt1 to trigger lethal autophagy in vivo. Thus, the results of the in vivo experiments are in accordance with those of in vitro experiments.

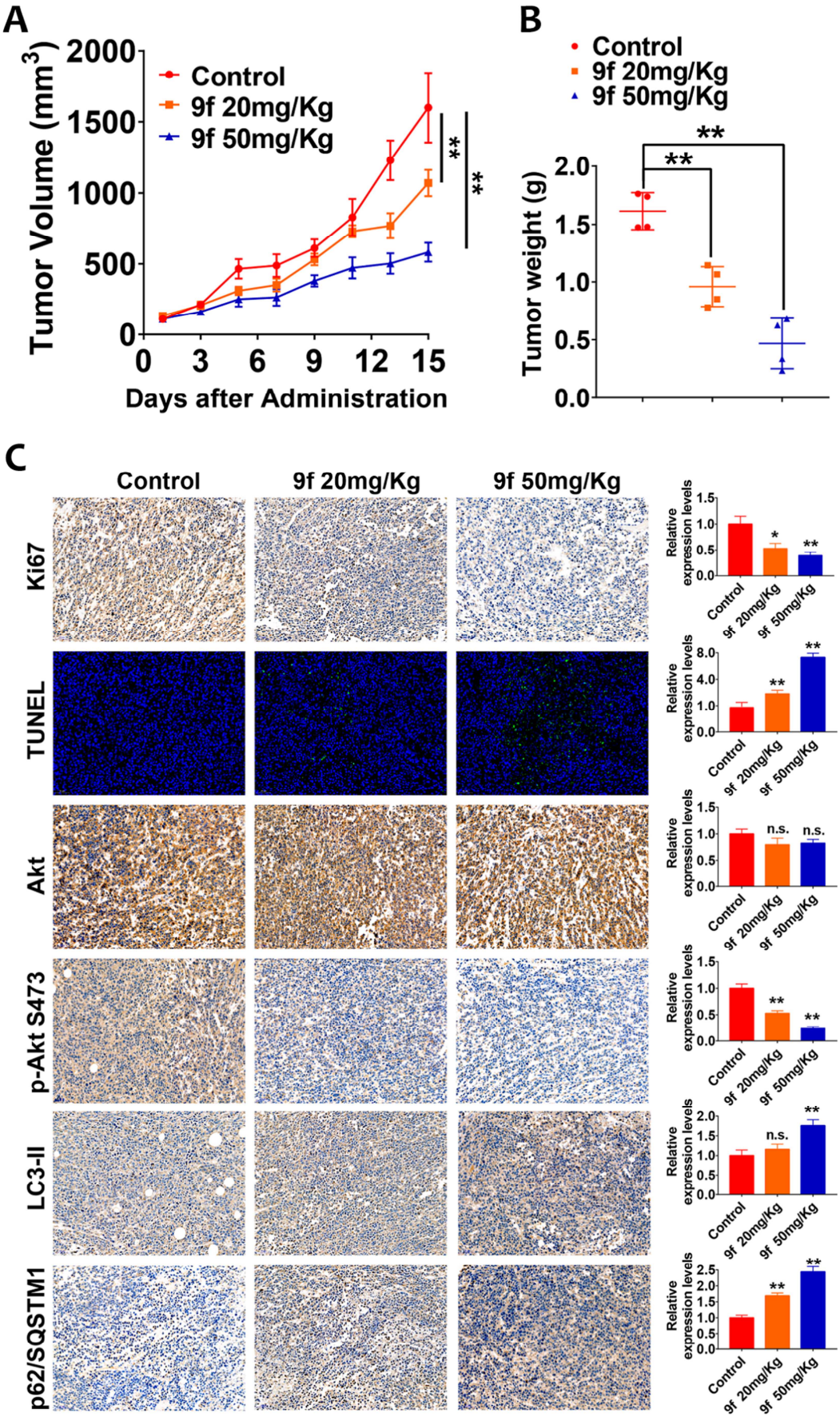
A
Tumor Volume (mm3)
2000
1500
1000
500
0
Control
9f 20mg/Kg
9f 50mg/Kg
**
**
0 3 6 9 12 15
Days after Administration
B
Control
9f 20mg/Kg
9f 50mg/Kg
**
**
Tumor weight (g)
2.0
1.5
1.0
0.5
0.0
C
Control
9f 20mg/Kg
9f 50mg/Kg
Ki67
TUNEL
Akt
p-Akt S473
LC3-II
p62/SQSTM1
Relative expression levels
n.s.
Control
9f 20mg/Kg
9f 50mg/Kg

Figure 6. Compound 9f suppressed the growth of Huh-7 xenograft models in vivo. (A) Changes in tumor volume in each group were determined from 1 to 15 days; (B) Analysis of the xenograft tumor tissue weight in each mouse in (A); (D) Protein expression levels of Ki67, TUNEL, total AKt, p-Akt (S473), LC3-II, and p62/SQSTM1 in each group were determined by IHC or IF. Scale bar: 50 μm.

In conclusion, we reported the design, synthesis and biological evaluation of the novel Akt1 inhibitors with the tricycle thieno[2,3-d]pyrimidine scaffold as a novel Akt1 inhibitor in the Huh-7 cells. The most potent compound **9f** remarkably suppressed the Huh-7 cell proliferation and induced lethal autophagy and apoptotic cell death. The detailed binding modes of **9f** to Akt1 were probed to elucidate its kinase selectivity. Furthermore, the antitumor capacity of **9f** was validated in the subcutaneous Huh-7 xenograft models. Collectively, these results indicate that **9f** suppressed the Huh-7 cell proliferation by inducing lethal autophagy mediated by the Akt/mTOR signaling pathway, suggesting novel molecular mechanism of these novel Akt inhibitors worthy for further study.

3. Experimental section

Reagents, Antibodies and Cell Cultures

GDC-0068, 3-MA and Bafilomycin-A1 were obtained from Selleckchem Co. Ltd. (Shanghai, China). The antibodies recognizing Bcl-2, Caspase-3, Caspase-9, Cytochrome C, LC-3, p62/SQSTM1 and GAPDH were purchased from Proteintech (Wuhan, China). The antibody recognizing Akt, p-Akt, mTOR and p-mTOR were purchased from Abcam (Cambridge, MA, USA). The malignant melanoma cell lines, including HepG2, Hep3B, Huh-7 and SMMC-7721 were obtained from the Chinese Center for Type Culture Collection (Wuhan, China) and cultured in DMEM (Dulbecco's modified Eagle's

medium) with 10% of FBS (fetal bovine serum) and streptomycin. The cytotoxicity assay was performed with MTT method as previously described.

Kinase inhibition assay

AKT1, AKT2, AKT3 and PKA kinase assay used the Kinase Profiler services supplied by Eurofins in the light of our previous report.[50-52] The KINOMEScan® selectivity profiling was implemented by DiscoveRx Co. Ltd. and on the baisis of the company's protocol.

Apoptosis and autophagy assay

The apoptosis of cells caused by the compound **9f** is tested by Annexin V/PI dual-staining flow cytometry method on SMMC-7721 cells. The experimental method and procedure have been described detailedly in our previous reports. And the autophagy assay is relied on SMMC-7721 cells transfected by GFP-LC3. Briefly speaking, the SMMC-7721 cells after transfecting are processed by saline or compound **9f** for 6 h, after that the cells are going to fix by paraformaldehyde and the phenomenon of autophagosome punctures can be observed through the accumulated of GFP-LC3.

Western Blotting analysis

For western blotting, the extracts of total protein from each sample were treated in accordance with the method we described previously. In short, the total proteins were loaded into the SDS-PAGE (sodium dodecyl sulfate-polyacrylamide) gel and separated through the different of their molecular weight in electrophoresis (PAGE), after that the separated proteins were shifted into a PVDF membrane and incubated through corresponding membrane react pathways. (Millipore, Burlington, MA, USA). The resulted membranes reacted with major antibodies and HRP (horseradish peroxidase)-conjugated secondary antibodies (1:10,000). The expression profiles of target proteins can be identified through an enhanced chemiluminescence (ECL) WB substrate (Millipore, MA. USA).

Animal models

The research on anti-tumor activity of **9f** in vivo was implemented based on the Guidelines for the Care. All animal experimental studies were authorized by the Animal Ethics Committee of Animal Experimentation of West China Hospital, Sichuan University. The 6-8 weeks old SPF (specific pathogen-free) nude mice were purchased from Beijing Huafukang Biotechnology Co., Ltd. The preliminary safety evaluation of the anti-tumor activity of **9f** in vivo was performed using the models of SMMC-7721 subcutaneous xenograft. SMMC-7721 cells, a single cell suspension (5×10^5/100 μL) in

PBS, were injected into the dorsal subcutaneous of mice. The size of the tumor was measured every two days from the time of injection. The volume of tumor is calculated in the light of Vol = $a \times b^2 \times 0.5$ (a, b represent the large and the small diameter tumor tissue, respectively). The tumor tissues were stripped, fixed with formalin, embedded in paraffin and sliced, after that the sections were stained by TUNEL, LC3-II, Akt, pAkt473 and Ki67 for further histological research.

Tissue microarray (TMA), Immunohistochemistry and Immunofluorescent assays

The histological sections of tumor tissue were immersed into EDTA antigen recovery buffer (pH 8.0) or citrate buffer (pH 6.0), and then microwave was used to recover antigen. Then the slide was incubated with the corresponding primary antibody at 37 °C for 30-40 minutes. Normal anti-rabbit or anti-mouse IgG was used as a negative control group. Immunohistochemical analysis was performed with diaminobenzidine solution after the sections was treated with HRP polymer as well as the second antibody for 30 minutes. Immunofluorescence (IF) test was carried out by treating slides with fluorescein combined with secondary antibody and detecting under fluorescence microscope. A human liver cancer TMA was purchased from Shanghai Outdo Biotech. The IHC staining method is to use the primary antibody of rabbit against p-akt1 s473, as we mentioned before, unless otherwise stated.

Chemical synthesis section.

The whole chemical reagents including anhydrous reagents were commercially available and used without further purification. The reactions were monitored using TLC purchasing from commercial company. The silica gel for column chromatography was buying from Qingdao Haiyang Chemical Co., Ltd (Pingdu, Qingdao, Shandong, China). ^{1}H NMR spectra were collected on a Bruker Avance III 400MHz apparatus and ^{13}C NMR data were measured at 100MHz in the same instrument. TMS (tetramethylsilane) was used as the internal standard and $CDCl_3$ was used to dissolve samples. The chemical shifts (δ) was marked in ppm. ESI-HRMS spectrum was collected using Waters TOF-MS instrument (Waters, Milford, MA, USA).

*2-(4-chlorophenyl)-3-(isopropylamino)-1-(4-(7-methyl-5,6,7,8-tetrahydropyrido[4',3':4,5]thieno[2 ,3-d]pyrimidin-4-yl)piperazin-1-yl)propan-1-one (**5a**)* as a white solid, m.p. 89.6-91.6 °C, yield 77%.

^{1}H NMR (400 MHz, $CDCl_3$) δ 8.49 (s, 1H), 7.32 (d, *J* = 8.4 Hz, 2H), 7.22 (d, *J* = 8.4 Hz, 2H), 4.06 (dd, *J* = 9.2, 5.2 Hz, 1H), 3.96 - 3.86 (m, 1H), 3.71 (s, 2H), 3.69 - 3.60 (m, 1H), 3.59 - 3.50 (m, 1H), 3.49 - 3.40 (m, 2H), 3.36 - 3.31 (m, 1H), 3.30 - 3.25 (m, 1H), 3.24 - 3.18 (m, 1H), 3.01 - 2.93 (m, 2H), 2.89 - 2.78 (m, 2H), 2.76 - 2.71 (m, 1H), 2.71 - 2.66 (m, 2H), 2.52 (s, 3H), 2.24 - 2.17 (m, 1H), 1.09 (d, *J* = 6.4 Hz, 3H), 1.05 (d, *J* = 6.4 Hz, 3H)**.** ^{13}C NMR (100 MHz, $CDCl_3$) δ 170.36, 168.78, 161.69, 151.75, 136.57, 133.46, 133.28, 129.41, 129.08, 124.78, 120.68, 52.26, 51.56, 50.52, 49.79, 49.29, 48.97, 45.59, 45.01, 41.53, 29.69, 27.34, 22.64, 22.58. HRMS: m/z calculated for $C_{26}H_{33}ClN_6OS$ $[M + Na]^+$: 535.2023, found: 535.2019.

*2-(4-chlorophenyl)-1-(4-(7-ethyl-5,6,7,8-tetrahydropyrido[4',3':4,5]thieno[2,3-d]pyrimidin-4-yl)piperazin-1-yl)-3-(isopropylamino)propan-1-one (**5b**)* as a white solid, m.p. 84.8-85.9 °C, yield 65%. ^{1}H NMR (400 MHz, $CDCl_3$) δ 8.47 (s, 1H), 7.30 (d, *J* = 8.4 Hz, 2H), 7.21 (d, *J* = 8.4 Hz, 2H), 4.09 (dd, *J* = 9.2, 5.2 Hz, 1H), 3.95 - 3.85 (m, 1H), 3.75 (s, 2H), 3.67 - 3.58 (m, 1H), 3.58 - 3.49 (m, 1H), 3.48 - 3.38 (m, 2H), 3.36 - 3.31 (m, 1H), 3.30 - 3.24 (m, 1H), 3.24 - 3.17 (m, 1H), 2.95 (s, 2H), 2.90 - 2.78 (m, 2H), 2.82 - 2.77 (m, 1H), 2.76 (d, *J* = 4.8 Hz, 1H), 2.72 (t, *J* = 5.6 Hz, 2H), 2.65 (q, *J* = 7.2 Hz, 2H), 1.19 (t, *J* = 7.2 Hz, 3H), 1.10 (d, *J* = 6.4 Hz, 3H), 1.06 (d, *J* = 6.4Hz, 3H). ^{13}C NMR (100 MHz, $CDCl_3$) δ 170.30, 168.79, 161.62, 151.70, 136.43, 133.51, 133.49, 129.43, 129.08, 125.14, 120.65, 52.38, 51.96, 51.42, 50.45, 50.23, 49.75, 49.10, 45.02, 41.55, 27.43, 22.48, 22.41, 12.43. HRMS: m/z calculated for $C_{27}H_{35}ClN_6OS$ $[M + Na]^+$: 549.2179, found: 549.2172.

*2-(4-chlorophenyl)-3-(isopropylamino)-1-(4-(7-propyl-5,6,7,8-tetrahydropyrido[4',3':4,5]thieno[2,3-d]pyrimidin-4-yl)piperazin-1-yl)propan-1-one (**5c**)* as a white solid, m.p. 79.5-81.6 °C, yield 70%. ^{1}H NMR (400 MHz,$CDCl_3$) δ 8.46 (s, 1H), 7.33 (d, *J* = 8.4 Hz, 2H), 7.22 (d, *J* = 8.4 Hz, 2H), 4.32 (br s, 1H), 4.27 (dd, *J* = 10.0, 4.4 Hz, 1H), 3.93 - 3.85 (m, 1H), 3.74 (s, 2H), 3.71 - 3.63 (m, 1H), 3.54 - 3.45

(m, 2H), 3.41 - 3.31 (m, 3H), 3.28 - 3.20 (m, 1H), 3.16 - 3.05 (m, 1H), 2.99 - 2.91 (m, 3H), 2.89 - 2.80 (m, 1H), 2.76 - 2.67 (m, 2H), 2.56 - 2.49 (m, 2H), 1.67 - 1.56 (m, 2H), 1.24 (d, *J* = 6.4 Hz, 3H), 1.22 (d, *J* = 6.4 Hz, 3H), 0.96 (t, *J* = 7.6 Hz, 3H). ^{13}C NMR (100 MHz, $CDCl_3$) δ 169.93, 168.77, 161.52, 151.64, 135.21, 134.05, 133.61, 129.71, 129.08, 125.23, 120.68, 60.09, 52.81, 50.59, 50.49, 50.33, 49.42, 47.64, 44.99, 41.66, 27.37, 21.23, 21.20, 20.46, 11.90. HRMS: m/z calculated for $C_{28}H_{37}ClN_6OS$ $[M + Na]^+$: 563.2336, found: 563.2327.

*1-(4-(7-benzyl-5,6,7,8-tetrahydropyrido[4',3':4,5]thieno[2,3-d]pyrimidin-4-yl)piperazin-1-yl)-2-(4-chlorophenyl)-3-(isopropylamino)propan-1-one (**5d**)* as a white solid, m.p. 77.7-87.2 °C, yield 66%. ^{1}H NMR (400 MHz, $CDCl_3$) δ 8.49 (s, 1H), 7.41 - 7.32 (m, 5H), 7.31 (d, *J* = 8.4 Hz, 2H), 7.23 (d, *J* = 8.4 Hz, 2H), 4.10 (dd, *J* = 9.2, 5.2 Hz, 1H), 3.96 - 3.86 (m, 1H), 3.74 (d, *J* = 3.2 Hz, 4H), 3.68 - 3.60 (m, 1H), 3.59 - 3.51 (m, 1H), 3.50 - 3.40 (m, 2H), 3.38 - 3.32 (m, 1H), 3.31 - 3.26 (m, 1H), 3.26 - 3.20 (m, 1H), 2.96 (t, *J* = 5.6 Hz, 2H), 2.88 - 2.80 (m, 2H), 2.80 - 2.76 (m, 2H), 2.73 (d, *J* = 5.2 Hz, 1H), 2.63 (br s, 1H), 1.11 (d, *J* = 6.3 Hz, 3H), 1.07 (d, *J* = 6.4 Hz, 3H). ^{13}C NMR (100 MHz, $CDCl_3$) δ 170.34, 168.81, 161.65, 151.68, 137.57, 136.50, 133.47, 133.45, 129.42, 129.11, 129.09, 128.49, 127.50, 125.17, 120.72, 62.44, 52.70, 51.48, 50.58, 50.18, 49.69, 49.13, 49.01, 45.01, 41.55, 27.36, 22.55, 22.48. HRMS: m/z calculated for $C_{32}H_{37}ClN_6OS$ $[M + H]^+$: 589.2516, found: 589.2512.

*2-(4-chlorophenyl)-1-(4-(7-cyclopropyl-5,6,7,8-tetrahydropyrido[4',3':4,5]thieno[2,3-d]pyrimidin-4-yl)piperazin-1-yl)-3-(isopropylamino)propan-1-one (**5e**)* as a white solid, m.p. 69.3-70.6 °C, yield 64%. ^{1}H NMR (400 MHz, $CDCl_3$) δ 8.41 (s, 1H), 7.24 (d, *J* = 8.4 Hz, 2H), 7.16 (d, *J* = 8.4 Hz, 2H), 3.94 (dd, *J* = 8.8, 4.8 Hz, 1H), 3.90 - 3.86 (m, 1H), 3.84 (s, 2H), 3.62 - 3.44 (m, 2H), 3.44 - 3.32 (m, 2H), 3.31 - 3.24 (m, 1H), 3.21 (m, 1H), 3.24 - 3.17 (m, 1H), 2.86 (t, *J* = 3.6 Hz, 4H), 2.80 - 2.69 (m, 2H), 2.65 (dd, *J* = 11.6, 5.2 Hz, 1H), 1.95 (br s, 1H), 1.85 - 1.78 (m, 1H), 1.00 (d, *J* = 6.4 Hz, 3H), 0.96

(d, *J* = 6.4 Hz, 3H), 0.54 - 0.45 (m, 4H). ^{13}C NMR (100 MHz, $CDCl_3$) δ 170.31, 168.71, 161.59, 151.58, 136.70, 133.33, 133.25, 129.27, 129.04, 125.01, 120.66, 52.68, 51.68, 50.54, 50.48, 49.69, 49.42, 48.73, 44.93, 41.45, 37.80, 27.16, 22.81, 22.75, 6.28. HRMS: m/z calculated for $C_{28}H_{35}ClN_6OS$ $[M + H]^+$: 539.2360, found: 539.2355.

2-(4-chlorophenyl)-1-(4-(7-isopropyl-5,6,7,8-tetrahydropyrido[4',3':4,5]thieno[2,3-d]pyrimidin-4-yl)piperazin-1-yl)-3-(isopropylamino)propan-1-one ***(5f)*** as a white solid, m.p. 65.2 - 67.0 °C, yield 55%. ^{1}H NMR (400 MHz, $CDCl_3$) δ 8.48 (s, 1H), 7.32 (d, *J* = 8.4 Hz, 2H), 7.23 (d, *J* = 8.4 Hz, 2H), 4.05 (dd, *J* = 8.8, 4.8 Hz, 1H), 3.96 - 3.88 (m, 1H), 3.85 (s, 2H), 3.70 - 3.60 (m, 1H), 3.59 - 3.51 (m, 1H), 3.51 - 3.40 (m, 2H), 3.40 - 3.33 (m, 1H), 3.32 - 3.26 (m, 1H), 3.26 - 3.20 (m, 1H), 3.00 - 2.92 (m, 3H), 2.90 - 2.80 (m, 2H), 2.80 - 2.72 (m, 3H), 2.58 (br s, 1H), 1.17 (s, 3H), 1.15 (s, 3H), 1.11 (d, *J* = 6.4 Hz, 3H), 1.07 (d, *J* = 6.4 Hz, 3H). ^{13}C NMR (100 MHz, $CDCl_3$) δ 170.28, 168.74, 161.50, 151.59, 136.45, 134.09, 133.44, 129.38, 129.07, 125.32, 120.64, 54.17, 51.50, 50.41, 49.64, 49.14, 49.08, 48.31, 46.20, 44.99, 41.54, 28.09, 22.53, 22.48, 18.54, 18.49. HRMS: m/z calculated for $C_{28}H_{37}ClN_6OS$ $[M + H]^+$: 541.2516, found: 541.2514.

2-(4-chlorophenyl)-3-(ethylamino)-1-(4-(7-methyl-5,6,7,8-tetrahydropyrido[4',3':4,5]thieno[2,3-d]pyrimidin-4-yl)piperazin-1-yl)propan-1-one ***(5g)*** as a white solid, m.p. 95.4-96.2 °C, yield 65%. ^{1}H NMR (400 MHz, $CDCl_3$) δ 8.48 (s, 1H), 7.30 (d, *J* = 8.4 Hz, 2H), 7.21 (d, *J* = 8.4 Hz, 2H), 4.05 (dd, *J* = 8.8, 5.2 Hz, 1H), 3.95 - 3.86 (m, 1H), 3.70 (s, 2H), 3.68 - 3.60 (m, 1H), 3.60 - 3.50 (m, 1H), 3.48 - 3.38 (m, 2H), 3.35 - 3.26 (m, 2H), 3.26 - 3.18 (m, 1H), 3.03 - 2.92 (m, 2H), 2.88 - 2.79 (m, 1H), 2.75 - 2.70 (m, 1H), 2.70 - 2.66 (m, 3H), 2.66 - 2.59 (m, 1H), 2.51 (s, 3H), 2.29 (s, 1H), 1.09 (t, *J* = 7.2 Hz, 3H). ^{13}C NMR (100 MHz, $CDCl_3$) δ 170.34, 168.77, 161.69, 151.74, 136.54, 133.41, 133.28, 129.38,

129.07, 124.77, 120.68, 54.63, 53.90, 52.25, 50.56, 49.80, 49.22, 45.59, 45.01, 44.19, 41.52, 27.34, 15.00. HRMS: m/z calculated for $C_{25}H_{31}ClN_6OS$ $[M + Na]^+$: 521.1866, found: 521.1859.

*3-(butylamino)-2-(4-chlorophenyl)-1-(4-(7-methyl-5,6,7,8-tetrahydropyrido[4',3':4,5]thieno[2,3-d]pyrimidin-4-yl)piperazin-1-yl)propan-1-one (**5h**)* as a white solid, m.p. 84.8-86.5 °C, yield 74%. ^{1}H NMR (400 MHz, $CDCl_3$) δ 8.47 (s, 1H), 7.29 (d, *J* = 8.4 Hz, 2H), 7.19 (d, *J* = 8.4 Hz, 2H), 4.04 (dd, *J* = 8.8, 5.2 Hz, 1H), 4.08 - 3.99 (m, 1H), 3.69 (s, 2H), 3.66 - 3.59 (m, 1H), 3.57 - 3.49 (m, 1H), 3.47 - 3.37 (m, 2H), 3.35 - 3.16 (m, 3H), 2.95 (t, *J* = 5.4 Hz, 2H), 2.87 - 2.77 (m, 1H), 2.71 (d, *J* = 5.2 Hz, 1H), 2.69 - 2.65 (m, 2H), 2.64 - 2.54 (m, 2H), 2.49 (s, 3H), 2.22 (s, 1H), 1.49 - 1.39 (m, 2H), 1.34 - 1.25 (m, 3H), 0.87 (t, *J* = 7.6 Hz, 3H). ^{13}C NMR (100 MHz, $CDCl_3$) δ 170.35, 168.75, 161.67, 151.72, 136.57, 133.37, 133.26, 129.35, 129.06, 124.77, 120.66, 54.61, 54.12, 52.24, 50.54, 49.80, 49.74, 49.21, 45.58, 45.00, 41.50, 31.94, 27.33, 20.39, 13.95. HRMS: m/z calculated for $C_{27}H_{35}ClN_6OS$ $[M + Na]^+$: 549.2179, found: 549.2170.

*N-(2-(4-chlorophenyl)-3-(4-(7-methyl-5,6,7,8-tetrahydropyrido[4',3':4,5]thieno[2,3-d]pyrimidin-4 -yl)piperazin-1-yl)but-3-en-1-yl)cyclopentanamine (**5i**)* as a white solid, m.p. 92.2-94.3 °C, yield 79%. ^{1}H NMR (400 MHz, $CDCl_3$) δ 8.47 (s, 1H), 7.29 (d, *J* = 8.4 Hz, 2H), 7.19 (d, *J* = 8.4 Hz, 2H), 4.04 (dd, *J* = 8.8, 5.2 Hz, 1H), 3.93 - 3.85 (m, 1H), 3.69 (d, *J* = 2.2 Hz, 2H), 3.67 - 3.57 (m, 1H), 3.57 - 3.48 (m, 1H), 3.47 - 3.38 (m, 2H), 3.34 - 3.17 (m, 3H), 3.09 - 3.01 (m, 1H), 2.98 - 2.92 (m, 2H), 2.86 - 2.76 (m, 1H), 2.71 - 2.64 (m, 3H), 2.50 (s, 3H), 2.33 (br s, 1H), 1.87 - 1.77 (m, 2H), 1.71 - 1.57 (m, 2H), 1.55 - 1.44 (m, 2H), 1.35 - 1.26 (m, 2H). ^{13}C NMR (100 MHz, $CDCl_3$) δ 170.37, 168.75, 161.67, 151.72, 136.67, 133.36, 133.25, 129.36, 129.07, 124.77, 120.65, 60.02, 54.62, 52.95, 52.24, 50.52, 49.79, 49.39, 45.58, 45.00, 41.50, 32.99, 32.79, 27.33, 24.05, 24.01. HRMS: m/z calculated for $C_{28}H_{35}ClN_6OS$ $[M + Na]^+$ 561.2179, found: 561.2177.

*2-(4-chlorophenyl)-3-(cyclohexylamino)-1-(4-(7-methyl-5,6,7,8-tetrahydropyrido[4',3':4,5]thieno[2,3-d]pyrimidin-4-yl)piperazin-1-yl)propan-1-one (**5j**)* as a white solid, m.p. 84.9-86.2 °C, yield 81%. ^{1}H NMR (400 MHz, $CDCl_3$) δ 8.50 (s, 1H), 7.31 (d, *J* = 8.4 Hz, 2H), 7.22 (d, *J* = 8.4 Hz, 2H), 4.06 (dd, *J* = 8.8, 5.2 Hz, 1H), 3.97 - 3.87 (m, 1H), 3.72 (s, 2H), 3.69 - 3.61 (m, 1H), 3.60 - 3.51 (m, 1H), 3.50 - 3.40 (m, 2H), 3.38 - 3.28 (m, 2H), 3.27 - 3.18 (m, 1H), 2.98 (s, 2H), 2.88 - 2.74 (m, 3H), 2.69 (t, *J* = 5.2 Hz, 2H), 2.52 (s, 3H), 2.49 - 2.42 (m, 1H), 1.94 - 1.82 (m, 2H), 1.76 - 1.66 (m, 2H), 1.64 - 1.56 (m, 1H), 1.24 - 1.21 (m, 1H), 1.20 - 1.12 (m, 2H), 1.12 - 1.01 (m, 2H). ^{13}C NMR (100 MHz, $CDCl_3$) δ 170.35, 168.74, 161.66, 151.71, 136.60, 133.38, 133.24, 129.34, 129.06, 124.77, 120.64, 56.97, 54.61, 52.24, 51.13, 50.50, 49.78, 49.35, 45.57, 44.99, 41.50, 33.21, 33.13, 27.33, 26.00, 24.95, 24.93. HRMS: m/z calculated for $C_{29}H_{37}ClN_6OS$ $[M + Na]^+$: 575.2336, found: 575.2328.

*2-(4-fluorophenyl)-3-(isopropylamino)-1-(4-(7-methyl-5,6,7,8-tetrahydropyrido[4',3':4,5]thieno[2,3-d]pyrimidin-4-yl)piperazin-1-yl)propan-1-one (**5k**)* as a white solid, m.p. 108.8-110.0 °C, yield 65%. ^{1}H NMR (400 MHz, $CDCl_3$) δ 8.48 (s, 1H), 7.28 (dd, *J* = 8.8, 5.4 Hz, 2H), 7.05 (t, *J* = 8.6 Hz, 2H), 4.42 (br s, 1H), 4.34 (dd, *J* = 9.2, 4.4 Hz, 1H), 3.99 - 3.89 (m, 1H), 3.72 (s, 2H), 3.69 - 3.61 (m, 1H), 3.60 - 3.52 (m, 1H), 3.52 - 3.41 (m, 2H), 3.36 (dd, *J* = 11.2, 9.2 Hz, 2H), 3.27 - 3.18 (m, 1H), 3.07 - 3.00 (m, 1H), 2.99 (t, *J* = 5.6 Hz, 2H), 2.88 (dd, *J* = 11.6, 4.8 Hz, 1H), 2.84 - 2.87 (m, 1H), 2.69 (t, *J* = 5.6 Hz, 2H), 2.52 (s, 3H), 1.21 (d, *J* = 6.4 Hz, 3H), 1.20 (d, *J* = 6.4 Hz, 3H). ^{13}C NMR (100 MHz, $CDCl_3$) δ 170.26, 168.70, 162.15(d, J_{CF} = 245.7 Hz), 161.63, 151.68, 133.24, 133.07(d, J_{CF} = 3.2 Hz), 129.36(d, J_{CF} = 7.9 Hz), 124.78, 120.64, 116.33(d, J_{CF} = 21.4 Hz), 54.59, 52.21, 50.73, 50.37, 49.71, 49.67, 47.95, 45.55, 45.02, 41.58, 27.29, 21.61, 21.55. HRMS: m/z calculated for $C_{26}H_{33}FN_6OS$ $[M + Na]^+$: 519.2318, found: 519.2311.

*2-(4-bromophenyl)-3-(isopropylamino)-1-(4-(7-methyl-5,6,7,8-tetrahydropyrido[4',3':4,5]thieno[2,3-d]pyrimidin-4-yl)piperazin-1-yl)propan-1-one (**5l**)* as a white solid, m.p. 78.0-79.5 °C, yield 75%. ^{1}H NMR (400 MHz, $CDCl_3$) δ 8.49 (s, 1H), 7.47 (d, *J* = 8.4 Hz, 2H), 7.16 (d, *J* = 8.4 Hz, 2H), 4.12 (dd, *J* = 8.8, 5.2 Hz, 1H), 3.94 - 3.86 (m, 1H), 3.71 (s, 2H), 3.69 - 3.61 (m, 1H), 3.59 - 3.50 (m, 1H), 3.48 - 3.40 (m, 2H), 3.37 - 3.32 (m, 1H), 3.32 - 3.25 (m, 2H), 3.24 - 3.18 (m, 1H), 2.96 (t, *J* = 5.6 Hz, 2H), 2.91 - 2.81 (m, 2H), 2.76 (dd, *J* = 11.6, 5.2 Hz, 1H), 2.69 (t, *J* = 5.6 Hz, 2H), 2.51 (s, 3H), 1.11 (d, *J* = 6.4 Hz, 3H), 1.08 (d, *J* = 6.4 Hz, 3H). ^{13}C NMR (100 MHz, $CDCl_3$) δ 170.25, 168.73, 161.65, 151.70, 137.15, 133.24, 132.31, 129.41, 124.77, 121.45, 120.64, 54.61, 52.23, 51.57, 50.49, 49.79, 49.44, 48.89, 45.57, 44.99, 41.50, 27.32, 22.71, 22.66. HRMS: m/z calculated for $C_{26}H_{33}BrN_6OS$ $[M + Na]^+$: 579.1518, found: 579.1515.

*3-(isopropylamino)-1-(4-(7-methyl-5,6,7,8-tetrahydropyrido[4',3':4,5]thieno[2,3-d]pyrimidin-4-yl)piperazin-1-yl)-2-(p-tolyl)propan-1-one (**5m**)* as a white solid, m.p. 95.6-98.2 °C, yield 74%. ^{1}H NMR (400 MHz, $CDCl_3$) δ 8.48 (s, 1H), 7.20 - 7.11 (m, 4H), 4.26 (dd, *J* = 9.6, 4.4 Hz, 1H), 4.00 - 3.92 (m, 1H), 3.87 (q, *J* = 7.2 Hz, 1H), 3.71 (s, 2H), 3.66 - 3.55 (m, 1H), 3.53 - 3.44 (m, 3H), 3.34 - 3.27 (m, 2H), 3.24 - 3.19 (m, 1H), 3.02 - 2.92 (m, 3H), 2.83 (dd, *J* = 11.6, 4.8 Hz, 1H), 2.79 - 2.71 (m, 1H), 2.71 - 2.65 (m, 2H), 2.52 (s, 3H), 2.32 (s, 3H), 1.17 (t, *J* = 6.8 Hz, 6H). ^{13}C NMR (100 MHz, $CDCl_3$) δ 170.70, 168.70, 161.69, 151.69, 137.51, 134.33, 133.16, 130.02, 127.55, 124.84, 120.62, 53.42, 52.25, 50.97, 50.27, 49.78, 49.54, 48.61, 45.58, 45.02, 41.52, 27.35, 21.80, 21.73, 21.06. HRMS: m/z calculated for $C_{27}H_{36}N_6OS$ $[M + Na]^+$: 515.2569, found: 515.2567.

*3-(isopropylamino)-2-(4-methoxyphenyl)-1-(4-(7-methyl-5,6,7,8-tetrahydropyrido[4',3':4,5]thieno[2,3-d]pyrimidin-4-yl)piperazin-1-yl)propan-1-one (**5n**)* as a white solid, m.p. 70.4-71.2 °C, yield 69%. ^{1}H NMR (400 MHz, $CDCl_3$) δ 8.43 (s, 1H), 7.15 (d, *J* = 8.4 Hz, 2H), 6.82 (d, *J* = 8.4 Hz, 2H), 4.08 (dd,

J = 8.8, 5.2 Hz, 1H), 3.98 - 3.88 (m, 1H), 3.79 - 3.70 (m, 3H), 3.66 (s, 2H), 3.62 - 3.51 (m, 2H), 3.50 - 3.39 (m, 3H), 3.32 - 3.22 (m, 2H), 3.20 - 3.12 (m, 1H), 2.92 (s, 2H), 2.91 - 2.84 (m, 1H), 2.80 - 2.67 (m, 2H), 2.65 (br s, 2H), 2.47 (s, 3H), 1.11 (d, *J* = 6.4 Hz, 3H), 1.07 (d, *J* = 6.4 Hz, 3H). ^{13}C NMR (100 MHz, $CDCl_3$) δ 170.82, 168.66, 161.69, 158.95, 151.67, 133.12, 129.56, 128.76, 124.82, 120.60, 114.64, 55.23, 54.59, 52.21, 51.20, 50.31, 49.82, 49.28, 48.42, 45.55, 44.98, 41.46, 27.30, 22.08, 22.02. HRMS: m/z calculated for $C_{27}H_{36}N_6NaO_2S$ $[M + Na]^+$: 531.2518, found: 531.2515.

*2-(2-chlorophenyl)-3-(isopropylamino)-1-(4-(7-methyl-5,6,7,8-tetrahydropyrido[4',3':4,5]thieno[2,3-d]pyrimidin-4-yl)piperazin-1-yl)propan-1-one (**5o**)* as a white solid, m.p. 127.4-129.5 ℃, yield 67%. ^{1}H NMR (400 MHz, $CDCl_3$) δ 8.48 (s, 1H), 7.44 - 7.39 (m, 1H), 7.32 - 7.28 (m, 1H), 7.27 - 7.18 (m, 2H), 4.50 (dd, *J* = 9.6, 4.0 Hz, 1H), 4.06 - 3.98 (m, 1H), 3.72 (s, 2H), 3.65 - 3.55 (m, 1H), 3.54 - 3.44 (m, 2H), 3.41 - 3.29 (m, 2H), 3.27 - 3.13 (m, 2H), 3.03 - 2.93 (m, 2H), 2.85 (p, *J* = 6.4 Hz, 1H), 2.77 - 2.62 (m, 4H), 2.53 (s, 3H), 2.26 (s, 1H), 1.10 (d, *J* = 6.4 Hz, 3H), 1.07 (d, *J* = 6.4 Hz, 3H). ^{13}C NMR (100 MHz, $CDCl_3$) δ 170.65, 168.72, 161.69, 151.70, 135.75, 133.19, 132.94, 129.91, 128.81, 128.64, 127.61, 124.80, 120.62, 54.63, 52.25, 50.29, 50.01, 49.92, 48.53, 46.31, 45.59, 44.77, 41.58, 27.35, 22.82, 22.77. HRMS: m/z calculated for $C_{26}H_{33}ClN_6OS$ $[M + Na]^+$: 535.2023, found: 535.2017.

*2-(4-chlorophenyl)-3-(isopropylamino)-1-(4-(5,6,7,8-tetrahydrobenzo[4,5]thieno[2,3-d]pyrimidin-4-yl)piperazin-1-yl)propan-1-one (**9a**)* as a white solid, m.p. 87.2-89.0 °C, yield 78%. ^{1}H NMR (400 MHz, $CDCl_3$) δ 8.49 (s, 1H), 7.32 (d, *J* = 8.4 Hz, 2H), 7.23 (d, *J* = 8.4 Hz, 2H), 4.07 (dd, *J* = 8.8, 5.2 Hz, 1H), 3.98 - 3.90 (m, 1H), 3.70 - 3.62 (m, 1H), 3.62 - 3.54 (m, 1H), 3.50 - 3.38 (m, 2H), 3.36 - 3.30 (m, 1H), 3.30 - 3.25 (m, 1H), 3.25 - 3.17 (m, 1H), 2.90 - 2.79 (m, 6H), 2.73 (dd, *J* = 11.6, 5.2 Hz, 1H), 2.06 (br s, 1H), 1.96 - 1.88 (m, 2H), 1.84 - 1.72 (m, 2H), 1.09 (d, *J* = 6.4 Hz, 3H), 1.06 (d, *J* = 6.4 Hz, 3H). ^{13}C NMR (100 MHz, $CDCl_3$) δ 170.37, 168.56, 161.66, 151.39, 136.64, 135.85, 133.41, 129.38,

129.08, 126.74, 121.47, 51.68, 50.81, 49.81, 49.33, 48.93, 45.00, 41.53, 26.58, 25.80, 22.91, 22.75, 22.72, 22.66. HRMS: m/z calculated for $C_{26}H_{32}ClN_5OS$ $[M + H]^+$: 498.2094, found: 498.2090.

*2-(4-chlorophenyl)-1-(4-(6,7-dihydro-5H-cyclopenta[4,5]thieno[2,3-d]pyrimidin-4-yl)piperazin-1-yl)-3-(isopropylamino)propan-1-one (**9b**)* as a white solid, m.p. 90.2-91.5 °C, yield 71%. ^{1}H NMR (400 MHz, $CDCl_3$) δ 8.41 (s, 1H), 7.33 (d, *J* = 8.4 Hz, 2H), 7.24 (d, *J* = 8.4 Hz, 2H), 4.34 (dd, *J* = 9.6, 4.4 Hz, 1H), 3.92 - 3.85 (m, 1H), 3.76 - 3.60 (m, 2H), 3.56 - 3.47 (m, 2H), 3.45 - 3.40 (m, 1H), 3.40 - 3.32 (m, 2H), 3.18 - 3.08 (m, 1H), 3.06 - 2.92 (m, 6H), 2.44 (p, *J* = 7.2 Hz, 2H), 1.27 (d, *J* = 6.4 Hz, 3H), 1.25 (d, *J* = 6.4 Hz, 3H). ^{13}C NMR (100 MHz, $CDCl_3$) δ 173.39, 169.93, 160.06, 151.31, 140.59, 135.24, 135.13, 134.08, 129.71, 129.10, 117.33, 50.47, 50.42, 49.04, 48.35, 47.50, 45.09, 41.86, 31.44, 29.82, 28.18, 21.09. HRMS: m/z calculated for $C_{25}H_{30}ClN_5OS$ $[M + Na]^+$: 506.1757, found: 506.1752.

*2-(4-chlorophenyl)-1-(4-(5,8-dihydro-6H-pyrano[4',3':4,5]thieno[2,3-d]pyrimidin-4-yl)piperazin-1-yl)-3-(isopropylamino)propan-1-one (**9c**)* as a white solid, m.p. 75.3-77.5 °C, yield 78%. ^{1}H NMR (400 MHz, $CDCl_3$) δ 8.49 (s, 1H), 7.30 (d, *J* = 8.4 Hz, 2H), 7.21 (d, *J* = 8.4 Hz, 2H), 4.88 (s, 2H), 3.98 (dd, *J* = 8.8, 5.2 Hz, 1H), 3.96 - 3.92 (m, 1H), 3.90 (t, *J* = 5.2 Hz, 2H), 3.68 - 3.51 (m, 2H), 3.50 - 3.40 (m, 2H), 3.38 - 3.31 (m, 1H), 3.30 - 3.22 (m, 2H), 2.94 (s, 2H), 2.89 - 2.80 (m, 1H), 2.78 (p, *J* = 6.4 Hz, 1H), 2.69 (dd, *J* = 11.6, 5.2 Hz, 1H), 1.77 (br s, 1H), 1.06 (d, *J* = 6.4 Hz, 3H), 1.01 (d, *J* = 6.4 Hz, 3H). ^{13}C NMR (100 MHz, $CDCl_3$) δ 170.42, 168.87, 161.57, 151.82, 136.74, 133.37, 133.07, 129.36, 129.07, 124.59, 120.42, 65.68, 64.79, 51.79, 50.52, 49.61, 48.80, 44.96, 41.49, 27.24, 22.90, 22.83. HRMS: m/z calculated for $C_{25}H_{30}ClN_5O_2S$ $[M + Na]^+$: 522.1706, found: 522.1703.

*2-(4-chlorophenyl)-1-(4-(6,7-dihydro-5H-cyclopenta[4,5]thieno[2,3-d]pyrimidin-4-yl)piperazin-1-yl)-3-(ethylamino)propan-1-one (**9d**)* as a white solid, m.p. 90.2-91.5 °C, yield 65%. ^{1}H NMR (400 MHz, $CDCl_3$) δ 8.42 (s, 1H), 7.30 (d, *J* = 8.4 Hz, 2H), 7.21 (d, *J* = 8.4 Hz, 2H), 4.03 (dd, *J* = 9.2, 5.6

Hz, 1H), 3.96 - 3.88 (m, 1H), 3.66 - 3.53 (m, 3H), 3.50 - 3.42 (m, 2H), 3.40 - 3.33 (m, 1H), 3.29 (dd, *J* = 12.0, 8.8 Hz, 1H), 3.02 - 2.92 (m, 5H), 2.73 - 2.57 (m, 3H), 2.48 - 2.38 (m, 2H), 1.90 (s, 1H), 1.08 (t, *J* = 6.8 Hz, 3H). ^{13}C NMR (100 MHz, $CDCl_3$) δ 173.40, 170.41, 160.15, 151.34, 140.53, 136.62, 135.21, 133.37, 129.34, 129.08, 117.34, 54.01, 49.47, 49.36, 48.45, 45.07, 44.21, 41.72, 31.46, 29.81, 28.16, 15.14. HRMS: m/z calculated for $C_{24}H_{28}ClN_5OS$ $[M + H]^+$: 470.1781, found: 470.1768.

3-(butylamino)-2-(4-chlorophenyl)-1-(4-(6,7-dihydro-5H-cyclopenta[4,5]thieno[2,3-d]pyrimidin-4-yl)piperazin-1-yl)propan-1-one ***(9e)*** as a white solid, m.p. 90.2-91.5 °C, yield 72%. ^{1}H NMR (400 MHz, $CDCl_3$) δ 8.41 (s, 1H), 7.34 (d, *J* = 8.4 Hz, 2H), 7.27 (d, *J* = 8.4 Hz, 2H), 4.90 (dd, *J* = 10.4, 4.0 Hz, 1H), 3.90 - 3.82 (m, 1H), 3.79 - 3.70 (m, 1H), 3.70 - 3.62 (m, 1H), 3.61 - 3.53 (m, 2H), 3.49 (t, *J* = 11.6 Hz, 1H), 3.46 - 3.39 (m, 1H), 3.38 - 3.31 (m, 1H), 3.15 (dd, *J* = 12.0, 4.0 Hz, 1H), 3.10 - 3.04 (m, 1H), 3.04 - 2.91 (m, 6H), 2.49 - 2.39 (m, 2H), 1.97 - 1.70 (m, 2H), 1.48 - 1.37 (m, 2H), 0.95 (t, *J* = 7.2 Hz, 3H). ^{13}C NMR (100 MHz, $CDCl_3$) δ 173.34, 169.42, 160.02, 151.27, 140.61, 135.21, 134.50, 134.14, 129.87, 129.13, 117.31, 51.28, 48.76, 48.51, 48.37, 45.72, 45.22, 42.02, 31.44, 29.80, 28.19, 28.14, 19.85, 13.49. HRMS: m/z calculated for $C_{26}H_{32}ClN_5OS$ $[M + Na]^+$: 520.1914, found 520.1912.

2-(4-chlorophenyl)-3-(cyclopentylamino)-1-(4-(6,7-dihydro-5H-cyclopenta[4,5]thieno[2,3-d]pyri midin-4-yl)piperazin-1-yl)propan-1-one ***(9f)*** as a white solid, m.p. 90.2-91.5 °C, yield 61%. ^{1}H NMR (400 MHz, $CDCl_3$) δ 8.43 (s, 1H), 7.32 (d, *J* = 8.4 Hz, 2H), 7.22 (d, *J* = 8.4 Hz, 2H), 4.03 (dd, *J* = 8.8, 5.2 Hz, 1H), 3.97 - 3.90 (m, 1H), 3.67 - 3.57 (m, 2H), 3.57 - 3.42 (m, 3H), 3.41 - 3.33 (m, 1H), 3.28 (dd, *J* = 11.6, 8.8 Hz, 1H), 3.07 (q, *J* = 6.8 Hz, 1H), 3.03 - 2.94 (m, 5H), 2.69 (dd, *J* = 11.6, 5.2 Hz, 1H), 2.49 - 2.40 (m, 2H), 1.86 - 1.80 (m, 2H), 1.72 - 1.60 (m, 2H), 1.57 - 1.46 (m, 2H), 1.39 - 1.24 (m, 3H). ^{13}C NMR (100 MHz, $CDCl_3$) δ 173.43, 170.47, 160.17, 151.37, 140.55, 136.76, 135.22, 133.36, 129.35,

129.08, 117.35, 60.04, 53.08, 49.58, 49.47, 48.45, 45.08, 41.72, 33.13, 32.93, 31.47, 29.83, 28.17, 24.07, 24.04. HRMS: m/z calculated for $C_{24}H_{28}ClN_5O$ $[M + Na]^+$: 532.1914, found: 532.1913.

*2-(4-chlorophenyl)-3-(cyclohexylamino)-1-(4-(6,7-dihydro-5H-cyclopenta[4,5]thieno[2,3-d]pyrimidin-4-yl)piperazin-1-yl)propan-1-one (**9g**)* as a white solid, m.p. 90.2-91.5 °C, yield 69%. ^{1}H NMR (400 MHz, $CDCl_3$) δ 8.43 (s, 1H), 7.31 (d, *J* = 8.4 Hz, 2H), 7.22 (d, *J* = 8.4 Hz, 2H), 4.00 (dd, *J* = 8.8, 5.2 Hz, 1H), 3.97 - 3.90 (m, 1H), 3.67 - 3.57 (m, 2H), 3.57 - 3.52 (m, 1H), 3.52 - 3.43 (m, 2H), 3.41 - 3.35 (m, 1H), 3.31 (dd, *J* = 11.6, 8.8 Hz, 1H), 3.04 - 2.91 (m, 5H), 2.74 (dd, *J* = 11.6, 5.2 Hz, 1H), 2.50 - 2.36 (m, 3H), 1.94 - 1.80 (m, 3H), 1.75 - 1.65 (m, 2H), 1.64 - 1.55 (m, 1H), 1.29 - 1.15 (m, 3H), 1.14 - 1.00 (m, 2H). ^{13}C NMR (100 MHz, $CDCl_3$) δ 173.42, 170.49, 160.17, 151.36, 140.53, 136.79, 135.22, 133.33, 129.32, 129.09, 117.34, 56.93, 51.34, 49.66, 49.47, 48.45, 45.08, 41.73, 33.51, 33.43, 31.47, 29.82, 28.17, 26.10, 25.04, 25.02. HRMS: m/z calculated for $C_{28}H_{34}ClN_5OS$ $[M + Na]^+$: 546.2070, found: 546.2067.

*1-(4-(6,7-dihydro-5H-cyclopenta[4,5]thieno[2,3-d]pyrimidin-4-yl)piperazin-1-yl)-2-(4-fluorophenyl)-3-(isopropylamino)propan-1-one (**9h**)* as a white solid, m.p. 90.2-91.5 °C, yield 73%. ^{1}H NMR (400 MHz, $CDCl_3$) δ 8.43 (s, 1H), 7.29 - 7.24 (m, 2H), 7.07 - 7.00 (m, 2H), 4.06 (dd, *J* = 8.8, 5.2 Hz, 1H), 3.99 - 3.92 (m, 1H), 3.67 - 3.58 (m, 2H), 3.56 - 3.44 (m, 3H), 3.40 - 3.32 (m, 1H), 3.29 (dd, *J* = 11.6, 8.8 Hz, 1H), 3.03 - 2.93 (m, 5H), 2.87 - 2.78 (m, 1H), 2.74 (dd, *J* = 11.6, 5.2 Hz, 1H), 2.49 - 2.39 (m, 2H), 2.11 (br s, 1H), 1.09 (d, *J* = 6.4 Hz, 3H), 1.05 (d, *J* = 6.4 Hz, 3H). ^{13}C NMR (100 MHz, $CDCl_3$) δ 173.41, 170.67, 162.03(d, JCF = 245.7 Hz), 160.17, 151.36, 140.52, 135.22, 133.91(d, J_{CF} = 3.2 Hz), 129.3(d, J_{CF} = 7.9 Hz), 117.34, 116.1(d, J_{CF} = 21.4 Hz), 51.78, 49.44, 49.25, 48.89, 48.44, 45.08, 41.71, 31.46, 29.82, 28.16, 22.76, 22.68. HRMS: m/z calculated for $C_{25}H_{30}FN_5OS$ $[M + Na]^+$: 490.2053, found: 490.2057.

1-(4-bromophenyl)-1-(4-(6,7-dihydro-5H-cyclopenta[4,5]thieno[2,3-d]pyrimidin-4-yl)piperazin-1-yl)-3-(isopropylamino)propan-1-one (***9i***) as a white solid, m.p. 90.2-91.5 °C, yield 61%. ^{1}H NMR (400 MHz, $CDCl_3$) δ 8.43 (s, 1H), 7.47 (d, *J* = 8.4 Hz, 2H), 7.17 (d, *J* = 8.4 Hz, 2H), 4.02 (dd, *J* = 8.8, 5.2 Hz, 1H), 3.97 - 3.85 (m, 1H), 3.68 - 3.59 (m, 2H), 3.57 - 3.44 (m, 3H), 3.41 - 3.34 (m, 1H), 3.28 (dd, *J* = 11.6, 8.8 Hz, 1H), 3.04 - 2.93 (m, 5H), 2.85 - 2.77 (m, 1H), 2.72 (dd, *J* = 11.6, 5.2 Hz, 1H), 2.49 - 2.40 (m, 2H), 1.89 (br s, 1H), 1.08 (d, *J* = 6.4 Hz, 3H), 1.04 (d, *J* = 6.4 Hz, 3H). ^{13}C NMR (100 MHz, $CDCl_3$) δ 173.44, 170.38, 160.17, 151.37, 140.55, 137.26, 135.22, 132.32, 129.44, 121.45, 117.35, 51.73, 49.66, 49.46, 48.81, 48.45, 45.09, 41.73, 31.48, 29.83, 28.18, 22.88, 22.81. HRMS: m/z calculated for $C_{25}H_{30}BrN_5OS$ $[M + Na]^+$: 550.1252, found: 550.1259.

1-(4-(6,7-dihydro-5H-cyclopenta[4,5]thieno[2,3-d]pyrimidin-4-yl)piperazin-1-yl)-3-(isopropylamino)-2-(4-methoxyphenyl)propan-1-one (***9j***) as a white solid, m.p. 90.2-91.5 °C, yield 63%. ^{1}H NMR (400 MHz, $CDCl_3$) δ 8.42 (s, 1H), 7.20 (d, *J* = 8.4 Hz, 2H), 6.87 (d, *J* = 8.4 Hz, 2H), 4.03 - 3.93 (m, 2H), 3.79 (s, 3H), 3.62 (m, 2H), 3.55 - 3.46 (m, 3H), 3.39 - 3.31 (m, 1H), 3.27 (dd, *J* = 11.6, 8.8 Hz, 1H), 3.02 - 2.94 (m, 4H), 2.93 - 2.86 (m, 1H), 2.86 - 2.78 (m, 1H), 2.73 (dd, *J* = 11.6, 5.2 Hz, 1H), 2.49 - 2.40 (m, 2H), 2.07 (s, 1H), 1.09 (d, *J* = 6.4 Hz, 3H), 1.05 (d, *J* = 6.4 Hz, 3H). ^{13}C NMR (100 MHz, $CDCl_3$) δ 173.37, 171.09, 160.20, 158.85, 151.36, 140.40, 135.28, 130.13, 128.77, 117.30, 114.56, 55.25, 51.82, 49.38, 49.20, 48.87, 48.48, 45.09, 41.66, 31.50, 29.81, 28.17, 22.77, 22.69. HRMS: m/z calculated for $C_{26}H_{33}N_5O_2S$ $[M + Na]^+$: 502.2253, found: 502.2255.

1-(2-chlorophenyl)-1-(4-(6,7-dihydro-5H-cyclopenta[4,5]thieno[2,3-d]pyrimidin-4-yl)piperazin-1-yl)-3-(isopropylamino)propan-1-one (***9k***) as a white solid, m.p. 90.2-91.5 °C, yield 71%. ^{1}H NMR (400 MHz, $CDCl_3$) δ 8.42 (s, 1H), 7.43 - 7.40 (m, 1H), 7.32 - 7.29 (m, 1H), 7.24 - 7.20 (m, 2H), 4.50 (dd, *J* = 9.6, 4.0 Hz, 1H), 4.05 - 3.97 (m, 1H), 3.67 - 3.54 (m, 2H), 3.53 - 3.44 (m, 2H), 3.42 - 3.29 (m,

2H), 3.23 (dd, *J* = 12.0, 9.6 Hz, 1H), 3.03 - 2.94 (m, 4H), 2.89 - 2.79 (m, 2H), 2.71 (dd, *J* = 12.0, 4.4 Hz, 1H), 2.49 - 2.39 (m, 2H), 1.80 (br s, 1H), 1.09 (d, *J* = 6.4 Hz, 3H), 1.06 (d, *J* = 6.4 Hz, 3H). ^{13}C NMR (100 MHz, $CDCl_3$) δ 173.40, 170.74, 160.19, 151.36, 140.47, 135.81, 135.26, 132.98, 129.90, 128.80, 128.66, 127.63, 117.33, 50.08, 49.36, 48.49, 46.44, 44.86, 41.81, 31.46, 29.82, 28.18, 22.92, 22.86. HRMS: m/z calculated for $C_{25}H_{30}ClN_5OS$ $[M + H]^+$: 484.1938, found: 484.1942.

4-(4-(2-(4-chlorophenyl)-3-(isopropylamino)propanoyl)piperazin-1-yl)-N,N-dimethyl-5,8-dihydro pyrido[4',3':4,5]thieno[2,3-d]pyrimidine-7(6H)-carboxamide ***(13)*** as a white solid, m.p. 89.2-91.6 °C, yield 74%. ^{1}H NMR (400 MHz, $CDCl_3$) δ 8.50 (s, 1H), 7.32 (d, *J* = 8.4 Hz, 2H), 7.23 (d, *J* = 8.4 Hz, 2H), 4.57 (s, 2H), 4.05 (dd, *J* = 8.8, 5.2 Hz, 1H), 3.98 - 3.90 (m, 1H), 3.69 - 3.55 (m, 2H), 3.54 - 3.47 (m, 2H), 3.47 - 3.41 (m, 2H), 3.41 - 3.33 (m, 1H), 3.32 - 3.22 (m, 2H), 3.03 (t, *J* = 5.6 Hz, 2H), 2.91 (s, 6H), 2.88 - 2.80 (m, 2H), 2.73 (dd, *J* = 11.6, 5.2 Hz, 1H), 2.14 (br s, 1H), 1.10 (d, *J* = 6.4 Hz, 3H), 1.06 (d, *J* = 6.4 Hz, 3H). ^{13}C NMR (101 MHz, $CDCl_3$) δ 170.39, 168.84, 164.33, 161.59, 151.88, 136.57, 133.43, 132.14, 129.40, 129.10, 125.99, 120.52, 51.64, 50.27, 49.83, 49.32, 48.93, 46.92, 44.98, 43.99, 41.49, 38.49, 26.54, 22.69, 22.62. HRMS: m/z calculated for $C_{28}H_{36}ClN_7O_2S$ $[M + H]^+$: 570.2418, found: 570.2416.

Acknowledgement

This work was supported by grants from National Natural Science Foundation of China (Grant No. 21772131 and 21472130), China Postdoctoral Science Foundation (No. 2016M602696 and 2016M592679), and the Fundamental Research Funds for the Science & Technology department of Sichuan Province (2019YFSY0004).

Supporting Information

Additional figures containing NMR spectra of synthesized compounds.

References

[1] Y.K. Cho, J.K. Kim, M.Y. Kim, H. Rhim, J.K. Han, Systematic review of randomized trials for hepatocellular carcinoma treated with percutaneous ablation therapies, Hepatology, 49 (2010) 453-459.
[2] D.Y. Ju, L.R. Roberts, Hepatocellular carcinoma: a global view, Nat Rev Gastroenterol Hepatol, 7 (2010) 448-458.
[3] M. Sherman, J. Bruix, M. Porayko, T. Tran, Screening for hepatocellular carcinoma: the rationale for the American Association for the Study of Liver Diseases recommendations, Hepatology, 56 (2012) 793-796.
[4] J. Best, C. Schotten, G. Lohmann, G. Gerken, A. Dechêne, Tivantinib for the treatment of hepatocellular carcinoma, Expert Opinion on Pharmacotherapy, 18 (2017) 727.
[5] C.R. de Lope, S. Tremosini, A. Forner, M. Reig, J. Bruix, Management of HCC, Journal of Hepatology, 56 (2012) S75-S87.
[6] P. Schirmacher, Strategies for hepatocellular carcinoma therapy and diagnostics: lessons learned from high throughput and profiling approaches, Hepatology, 53 (2011) 2112-2121.
[7] B. Xie, D.H. Wang, S.J. Spechler, Sorafenib for the Treatment of Hepatocellular Carcinoma: A Systematic Review, Digestive Diseases & Sciences, 57 (2012) 1122-1129.
[8] B.D. Manning, L.C. Cantley, AKT/PKB Signaling: Navigating Downstream, Cell, 129 (2007) 1261-1274.
[9] F. Meier, B. Schittek, S. Busch, C. Garbe, K. Smalley, K. Satyamoorthy, G. Li, M. Herlyn, The RAS/RAF/MEK/ERK and PI3K/AKT signaling pathways present molecular targets for the effective treatment of advanced melanoma, Frontiers in Bioscience A Journal & Virtual Library, 10 (2005) 2986-3001.
[10] C.S. Mitsiades, N. Mitsiades, M. Koutsilieris, The Akt pathway: molecular targets for anti-cancer drug development, Current Cancer Drug Targets, 4 (2004) 235-256.
[11] T.F. Franke, PI3K/Akt: getting it right matters, Oncogene, 27 (2008) 6473-6488.
[12] M.P. Scheid, J.R. Woodgett, PKB/AKT: functional insights from genetic models, Nature Reviews Molecular Cell Biology, 2 (2001) 760-768.
[13] D.A. Altomare, J.R. Testa, Perturbations of the AKT signaling pathway in human cancer, Oncogene, 24 (2005) 7455-7464.
[14] C. Garcia-Echeverria, W.R. Sellers, Drug discovery approaches targeting the PI3K/Akt pathway in cancer, Oncogene, 27 (2008) 5511-5526.
[15] A. Bellacosa, C.C. Kumar, A.D. Cristofano, J.R. Testa, Activation of AKT Kinases in Cancer: Implications for Therapeutic Targeting, Advances in Cancer Research, 94 (2005) 29-86.
[16] G. Song, G. Ouyang, S. Bao, The activation of Akt/PKB signaling pathway and cell survival, Journal of Cellular and Molecular Medicine, 9 (2005) 59-71.
[17] M. Yoeli-Lerner, A. Toker, Akt/PKB signaling in cancer: a function in cell motility and invasion, Cell Cycle, 5 (2006) 603-605.
[18] J.S. de Bono, U. De Giorgi, D.N. Rodrigues, C. Massard, S. Bracarda, A. Font, J.A. Arranz Arija,

K.C. Shih, G.D. Radavoi, N. Xu, W.Y. Chan, H. Ma, S. Gendreau, R. Riisnaes, P.H. Patel, D.J. Maslyar, V. Jinga, Randomized Phase II Study Evaluating Akt Blockade with Ipatasertib, in Combination with Abiraterone, in Patients with Metastatic Prostate Cancer with and without PTEN Loss, Clinical Cancer Research, 25 (2019) 928-936.

[19] P. Schmid, J. Abraham, S. Chan, D. Wheatley, M. Brunt, G. Nemsadze, R. Baird, Y.H. Park, P. Hall, T. Perren, R.C. Stein, M. László, J.-M. Ferrero, M. Phillips, J. Conibear, S.-J. Sarker, A. Prendergast, H. Cartwright, K. Mousa, N.C. Turner, AZD5363 plus paclitaxel versus placebo plus paclitaxel as first-line therapy for metastatic triple-negative breast cancer (PAKT): A randomised, double-blind, placebo-controlled, phase II trial, Journal of Clinical Oncology, 36 (2018) 1007-1007.

[20] D.A. Altomare, L. Zhang, J. Deng, A. Di Cristofano, A.J. Klein-Szanto, R. Kumar, J.R. Testa, GSK690693 Delays Tumor Onset and Progression in Genetically Defined Mouse Models Expressing Activated Akt, Clinical Cancer Research, 16 (2010) 486-496.

[21] C. Aghajanian, K.M. Bell-McGuinn, H.A. Burris, L.L. Siu, L.-A. Stayner, J.J. Wheler, D.S. Hong, C. Kurkjian, S. Pant, A. Santiago-Walker, J.L. Gauvin, J.M. Antal, J.B. Opalinska, S.R. Morris, J.R. Infante, A phase I, open-label, two-stage study to investigate the safety, tolerability, pharmacokinetics, and pharmacodynamics of the oral AKT inhibitor GSK2141795 in patients with solid tumors, Investigational New Drugs, 36 (2018) 1016-1025.

[22] C.X. Ma, V. Suman, M.P. Goetz, D.W. Northfelt, M.E. Burkard, F. Ademuyiwa, M.J. Naughton, J. Margenthaler, R. Aft, R.J. Gray, A Phase II trial of neoadjuvant MK2206, an AKT inhibitor, with anastrozole in clinical stage 2 or 3 PIK3CA mutant ER positive and HER2 negative breast cancer, Clinical Cancer Research, 23 (2017) 6823–6832.

[23] A. Colaprico, T.C. Silva, C. Olsen, L. Garofano, C. Cava, D. Garolini, T.S. Sabedot, T.M. Malta, S.M. Pagnotta, I. Castiglioni, M. Ceccarelli, G. Bontempi, H. Noushmehr, TCGAbiolinks: an R/Bioconductor package for integrative analysis of TCGA data, Nucleic acids research, 44 (2016) e71.

[24] J. Liu, T. Lichtenberg, K.A. Hoadley, L.M. Poisson, A.J. Lazar, A.D. Cherniack, A.J. Kovatich, C.C. Benz, D.A. Levine, A.V. Lee, L. Omberg, D.M. Wolf, C.D. Shriver, V. Thorsson, N. Cancer Genome Atlas Research, H. Hu, An Integrated TCGA Pan-Cancer Clinical Data Resource to Drive High-Quality Survival Outcome Analytics, Cell, 173 (2018) 400-416 e411.

[25] Z. Tang, C. Li, B. Kang, G. Gao, C. Li, Z. Zhang, GEPIA: a web server for cancer and normal gene expression profiling and interactive analyses, Nucleic acids research, 45 (2017) W98-W102.

[26] E.L. Huttlin, M.P. Jedrychowski, J.E. Elias, T. Goswami, R. Rad, S.A. Beausoleil, J. Villen, W. Haas, M.E. Sowa, S.P. Gygi, A tissue-specific atlas of mouse protein phosphorylation and expression, Cell, 143 (2010) 1174-1189.

[27] I. Khan, K.R. Garikapati, A. Setti, A.B. Shaik, V.K. Kanth Makani, M.A. Shareef, H. Rajpurohit, N. Vangara, M. Pal-Bhadra, A. Kamal, C.G. Kumar, Design, synthesis, in silico pharmacokinetics prediction and biological evaluation of 1,4-dihydroindeno[1,2-c]pyrazole chalcone as EGFR /Akt pathway inhibitors, European journal of medicinal chemistry, 163 (2019) 636-648.

[28] A. Viswanathan, D. Kute, A. Musa, S. Konda Mani, V. Sipila, F. Emmert-Streib, F.I. Zubkov, A.V. Gurbanov, O. Yli-Harja, M. Kandhavelu, 2-(2-(2,4-dioxopentan-3-ylidene)hydrazineyl)benzonitrile as novel inhibitor of receptor tyrosine kinase and PI3K/AKT/mTOR signaling pathway in glioblastoma, European journal of medicinal chemistry, 166 (2019) 291-303.

[29] W. Zhan, J. Che, L. Xu, Y. Wu, X. Hu, Y. Zhou, G. Cheng, Y. Hu, X. Dong, J. Li, Discovery of pyrazole-thiophene derivatives as highly Potent, orally active Akt inhibitors, European journal of medicinal chemistry, 180 (2019) 72-85.

[30] K. Lin, J. Lin, W.I. Wu, J. Ballard, B.B. Lee, S.L. Gloor, G.P. Vigers, T.H. Morales, L.S. Friedman, N. Skelton, B.J. Brandhuber, An ATP-site on-off switch that restricts phosphatase accessibility of Akt, Science signaling, 5 (2012) ra37.

[31] B.S. Lauber, L.A. Hardegger, A.K. Asraful, B.A. Lund, O. Dumele, M. Harder, B. Kuhn, R.A. Engh, F. Diederich, Addressing the Glycine-Rich Loop of Protein Kinases by a Multi-Facetted Interaction Network: Inhibition of PKA and a PKB Mimic, Chemistry, 22 (2016) 211-221.

[32] D. Chen, C.K. Soh, W.H. Goh, H. Wang, Design, Synthesis, and Preclinical Evaluation of Fused Pyrimidine-Based Hydroxamates for the Treatment of Hepatocellular Carcinoma, Journal of medicinal chemistry, 61 (2018) 1552-1575.

[33] H. Hobbs, G. Bravi, I. Campbell, M. Convery, H. Davies, G. Inglis, S. Pal, S. Peace, J. Redmond, D. Summers, Discovery of 3-Oxabicyclo[4.1.0]heptane, a Non-nitrogen Containing Morpholine Isostere, and Its Application in Novel Inhibitors of the PI3K-AKT-mTOR Pathway, Journal of medicinal chemistry, 62 (2019) 6972-6984.

[34] Y. Liu, Y. Yin, Z. Zhang, C.J. Li, H. Zhang, D. Zhang, C. Jiang, K. Nomie, L. Zhang, M.L. Wang, G. Zhao, Structural optimization elaborates novel potent Akt inhibitors with promising anticancer activity, European journal of medicinal chemistry, 138 (2017) 543-551.

[35] D. Yao, Y. Zhou, L. Zhu, L. Ouyang, J. Zhang, Y. Jiang, Y. Zhao, D. Sun, S. Yang, Y. Yu, J. Wang, Design, synthesis and structure-activity relationship studies of a focused library of pyrimidine moiety with anti-proliferative and anti-metastasis activities in triple negative breast cancer, European journal of medicinal chemistry, 140 (2017) 155-171.

[36] L. Ouyang, L. Zhang, J. Liu, L. Fu, D. Yao, Y. Zhao, S. Zhang, G. Wang, G. He, B. Liu, Discovery of a Small-Molecule Bromodomain-Containing Protein 4 (BRD4) Inhibitor That Induces AMP-Activated Protein Kinase-Modulated Autophagy-Associated Cell Death in Breast Cancer, Journal of Medicinal Chemistry, 60 (2017) 9990-10012.

[37] M. Zhang, L. Jiang, J. Tao, Z. Pan, M. He, D. Su, G. He, Q. Jiang, Design, synthesis and biological evaluation of 4-aniline-thieno[2,3-d]pyrimidine derivatives as MNK1 inhibitors against renal cell carcinoma and nasopharyngeal carcinoma, Bioorganic & Medicinal Chemistry, 27 (2019) 2268-2279.

[38] J.C. Aponte, A.J. Vaisberg, D. Castillo, G. Gonzalez, Y. Estevez, J. Arevalo, M. Quiliano, M. Zimic, M. Verástegui, E. Málaga, R.H. Gilman, J.M. Bustamante, R.L. Tarleton, Y. Wang, S.G. Franzblau, G.F. Pauli, M. Sauvain, G.B. Hammond, Trypanoside, anti-tuberculosis, leishmanicidal, and cytotoxic activities of tetrahydrobenzothienopyrimidines, Bioorganic & Medicinal Chemistry, 18 (2010) 2880-2886.

[39] K. Gewald, E. Schinke, H. Böttcher, Heterocyclen aus CH-aciden Nitrilen, VIII. 2-Amino-thiophene aus methylenaktiven Nitrilen, Carbonylverbindungen und Schwefel, Chemische Berichte, 99 (1966) 94-100.

[40] T.J. Fyfe, B. Kellam, S.N. Mistry, P.J. Scammells, J.R. Lane, B. Capuano, Subtle modifications to a thieno[2,3-d]pyrimidine scaffold yield negative allosteric modulators and agonists of the dopamine D2 receptor, European Journal of Medicinal Chemistry, 168 (2019) 474-490.

[41] J.F. Blake, N.C. Kallan, D. Xiao, R. Xu, J.R. Bencsik, N.J. Skelton, K.L. Spencer, I.S. Mitchell, R.D. Woessner, S.L. Gloor, T. Risom, S.D. Gross, M. Martinson, T.H. Morales, G.P.A. Vigers, B.J. Brandhuber, Discovery of pyrrolopyrimidine inhibitors of Akt, Bioorganic & Medicinal Chemistry Letters, 20 (2010) 5607-5612.

[42] C.-H. Wu, M.S. Coumar, C.-Y. Chu, W.-H. Lin, Y.-R. Chen, C.-T. Chen, H.-Y. Shiao, S. Rafi, S.-Y.

Wang, H. Hsu, C.-H. Chen, C.-Y. Chang, T.-Y. Chang, T.-W. Lien, M.-Y. Fang, K.-C. Yeh, C.-P. Chen, T.-K. Yeh, S.-H. Hsieh, J.T.A. Hsu, C.-C. Liao, Y.-S. Chao, H.-P. Hsieh, Design and Synthesis of Tetrahydropyridothieno[2,3-d]pyrimidine Scaffold Based Epidermal Growth Factor Receptor (EGFR) Kinase Inhibitors: The Role of Side Chain Chirality and Michael Acceptor Group for Maximal Potency, Journal of Medicinal Chemistry, 53 (2010) 7316-7326.

[43] X. Li, F.Y. Chen, J.W. Kang, J. Zhou, C. Peng, W. Huang, M.K. Zhou, G. He, B. Han, Stereoselective Assembly of Multifunctional Spirocyclohexene Pyrazolones That Induce Autophagy-Dependent Apoptosis in Colorectal Cancer Cells, The Journal of organic chemistry, 84 (2019) 9138-9150.

[44] Z. Pan, Y. Chen, J. Liu, Q. Jiang, S. Yang, L. Guo, G. He, Design, synthesis, and biological evaluation of polo-like kinase 1/eukaryotic elongation factor 2 kinase (PLK1/EEF2K) dual inhibitors for regulating breast cancer cells apoptosis and autophagy, European journal of medicinal chemistry, 144 (2018) 517-528.

[45] X. Wang, F. Wu, G. Li, N. Zhang, X. Song, Y. Zheng, C. Gong, B. Han, G. He, Lipid-modified cell-penetrating peptide-based self-assembly micelles for co-delivery of narciclasine and siULK1 in hepatocellular carcinoma therapy, Acta biomaterialia, 74 (2018) 414-429.

[46] Y. Wang, X. Wen, N. Zhang, L. Wang, D. Hao, X. Jiang, G. He, Small-molecule compounds target paraptosis to improve cancer therapy, Biomedicine & pharmacotherapy, 118 (2019) 109203.

[47] H. Chang, X. Li, Q. Cai, C. Li, L. Tian, J. Chen, X. Xing, Y. Gan, W. Ouyang, Z. Yang, The PI3K/Akt/mTOR pathway is involved in CVB3-induced autophagy of HeLa cells, International journal of molecular medicine, 40 (2017) 182-192.

[48] B. Ke, M. Tian, J. Li, B. Liu, G. He, Targeting Programmed Cell Death Using Small-Molecule Compounds to Improve Potential Cancer Therapy, Medicinal research reviews, 36 (2016) 983-1035.

[49] S. Matsuzaki, J.L. Pouly, M. Canis, In vitro and in vivo effects of MK2206 and chloroquine combination therapy on endometriosis: autophagy may be required for regrowth of endometriosis, British journal of pharmacology, 175 (2018) 1637-1653.

[50] D. Hao, X. Wen, L. Liu, L. Wang, X. Zhou, Y. Li, X. Zeng, G. He, X. Jiang, Sanshool improves UVB-induced skin photodamage by targeting JAK2/STAT3-dependent autophagy, Cell death & disease, 10 (2019) 19.

[51] X. Li, L. Yang, C. Peng, X. Xie, H.J. Leng, B. Wang, Z.W. Tang, G. He, L. Ouyang, W. Huang, B. Han, Organocatalytic tandem Morita-Baylis-Hillman-Michael reaction for asymmetric synthesis of a drug-like oxa-spirocyclic indanone scaffold, Chemical communications, 49 (2013) 8692-8694.

[52] R. Zhou, Q. Wu, M. Guo, W. Huang, X. He, L. Yang, F. Peng, G. He, B. Han, Organocatalytic cascade reaction for the asymmetric synthesis of novel chroman-fused spirooxindoles that potently inhibit cancer cell proliferation, Chemical communications, 51 (2015) 13113-13116.

Highlights

- 27 compounds were designed as novel Akt1 inhibitors and synthesized and tested for their anti-hepatocellular carcinoma activity.
- Compound 9f showed significant cytotoxicity with IC_{50} at nanomolar level both in kinase inhibitory and cell proliferation assays.
- Compound 9f induces lethal autophagy in Huh-7 cells both in vitro and in vivo.

Competing interests

The authors declare no competing interests.